

Halogen behaviour in subduction zones: Eclogite facies rocks from the Western and Central Alps

Lewis Hughes^{a,*}, Ray Burgess^a, Déborah Chavrit^{a,b}, Alison Pawley^a,
Romain Tartèse^a, Giles Droop^a, Chris J. Ballentine^c, Ian Lyon^a

^a School of Earth and Environmental Sciences, University of Manchester, Manchester M13 9PL, United Kingdom

^b Institut de Physique du Globe de Paris, Sorbonne Paris Cité, Univ Paris Diderot, CNRS, F-75005 Paris, France

^c Department of Earth Sciences, University of Oxford, South Parks Road, Oxford OX1 3AN, United Kingdom

Received 24 April 2018; accepted in revised form 22 September 2018; available online 28 September 2018

Abstract

We examined F, Cl, Br and I concentrations and distributions in eclogite facies rocks and minerals from the Western and Central Alpine ophiolitic zone to determine halogen behaviour in subduction zones, and to identify potential host phases that may be able to transport halogens to the deeper mantle. Analysis was carried out on a range of ophiolitic lithologies — peridotites, serpentinites, metagabbros, metabasalts and metasediments — to assess the distribution of halogens within deeply subducted oceanic crust. Halogen abundances in individual mineral phases range from below detection (~100 ppm) to ~1900 ppm for F, ~1 to ~3000 ppm for Cl, ~1 to ~11,000 ppb for Br and from <1 to ~1300 ppb for I. Bulk rock estimates of Cl, Br and I abundances are variable, but are generally more than one order of magnitude lower than those in altered oceanic crust (AOC), suggesting major halogen loss prior to or during eclogite facies metamorphism. Fluorine, however, can be enriched within metabasalts and metasediments, relative to the heavy halogens, suggesting F can be retained at eclogite facies conditions within the upper layers of the subducting slab. Bulk rock estimates suggest that upon reaching eclogite facies, the subducting slab has lost over 90% Cl, Br and I. Bromine and iodine concentrations show positive correlation, suggesting that they exhibit similar behaviour at high pressure. A lack of any other correlations suggest that F and Cl behave differently to Br and I during subduction. Elevated F/Cl, Br/Cl and I/Cl ratios, relative to AOC, suggest the preferential loss of Cl during shallower depths of subduction. *In situ* analyses and chemical mapping using electron probe micro-analysis and time of flight secondary ion mass spectrometry indicate that measured halogen abundances are primarily hosted within the mineral structure. Overall, our dataset provides new constraints on the available inventory of halogens that can be transferred to the deeper mantle via the subduction of oceanic crust.

© 2018 The Authors. Published by Elsevier Ltd. This is an open access article under the CC BY license (<http://creativecommons.org/licenses/by/4.0/>).

Keywords: Fluorine; Chlorine; Bromine; Iodine; Subduction; Eclogite; Alps

1. INTRODUCTION

The halogens — fluorine (F), chlorine (Cl), bromine (Br) and iodine (I) — are elements that exhibit increasingly incompatible and volatile behaviour from F to I. These properties make them useful tracers with which to investi-

gate global volatile recycling processes operating within the Earth's mantle (Schilling et al., 1980; Ito et al., 1983) and its various reservoirs, such as mantle minerals, silicate melts and aqueous fluids. Until relatively recently, analytical limitation in measuring the ppb-levels of Br and I within natural mineral assemblages has held back progress in understanding halogen behaviour in subduction zones. Previous studies have focused primarily on serpentinites and blueschists, on the behaviour of Cl during subduction (Ito

* Corresponding author.

E-mail address: lewis.hughes@manchester.ac.uk (L. Hughes).

et al., 1983; Philippot et al., 1998; John et al., 2010; Kendrick et al., 2011; Pagé et al., 2016; Pagé and Hattori, 2017; Kendrick et al., 2018), and on the nature of slab-derived fluids (Sumino et al., 2010; Kobayashi et al., 2017). Recent progress relates to advances in neutron irradiation noble gas mass spectrometry (NI-NGMS) (Kendrick, 2012a; Ruzié-Hamilton et al., 2016), which is providing unparalleled levels of detection for Cl, Br and I within mineral phases, in just milligram sized samples (Sumino et al., 2010; Kendrick et al., 2013; Kendrick et al., 2015a; Kendrick et al., 2015b; Kobayashi et al., 2017; Kendrick et al., 2018). This progress in noble gas and halogen analysis provides a means of addressing questions regarding the mechanisms of volatile retention, distribution and evolution within planetary interiors through geological time.

The incompatible nature of volatile elements during volcanic and magmatic processes leads to their depletion from the mantle and their enrichment in the crust (Hilton et al., 2002). Previous studies have attempted to constrain the halogen budget of the primitive mantle, and of MORB and OIB source regions, through various analytical and experimental means (e.g. Schilling et al., 1980; Deruelle et al., 1992; Jambon et al., 1995; Saal et al., 2002; Lyubetskaya and Korenaga, 2007; Joachim et al., 2015; Roberge et al., 2015; Joachim et al., 2017; Kendrick et al., 2017; Roberge et al., 2017). Whilst there is some disagreement on absolute abundances, it is accepted that concentrations of halogens in the mantle are low. However, despite low abundances in the mantle, appreciable concentrations of halogens have been measured in upper mantle diamonds derived from kimberlites (Burgess et al., 2002) and in Samoan mantle plume basalt samples (Kendrick et al., 2015a), and halogens are one of the most abundant volatile components to be emitted in mantle-derived arc magmas, after H₂O, S and CO₂ (Symonds et al., 1994; Aiuppa et al., 2009). The presence of halogens within these mantle-derived samples suggests that either the process of mantle degassing is not yet complete, or that there is a return flux of halogens to the mantle that influences its chemical evolution through time. The processes responsible for the return of halogen elements to the mantle are found at subduction zones; these are tectonic sites where volatile-rich crustal material can potentially be recycled back into the depleted mantle (e.g. Straub and Layne, 2003; Sumino et al., 2010; Kendrick et al., 2011; Kendrick et al., 2013; Kendrick et al., 2017).

Throughout subduction, as temperature and pressure increases, fluid phases and, if the geotherm is sufficiently warm, partial melts, are released during the breakdown of H₂O-rich slab components. The depth at which this breakdown occurs is dependent on both the geothermal gradient of the subduction zone, and the respective pressure-temperature-composition (P-T-X) stability of hydrous mineral phases. Given the incompatible and fluid mobile nature of the halogens, it is expected that they will be stripped from the descending slab during dehydration reactions. Hydrous minerals, however, have individual stability fields that span across large ranges of pressure and temperature space. These stability fields are further extended by halogen incor-

poration, most notably F, which can dramatically increase the stability of hydrous minerals, through F—OH substitution within the mineral structure (e.g. Holloway and Ford, 1975; Ulmer and Trommsdorff, 1999), especially within the Mg-rich end members of ferromagnesian solid solution systems. The increased compatibility of F in hydrous mineral phases, relative to Cl, Br and I, and its concomitant effects on thermal stability thus have a profound effect on the retention of F in descending slabs during the subduction process. Straub and Layne (2003) have estimated that only ~4–6% of F is returned to the surface via the mantle wedge through volcanic arc outflux. This contrasts with the heavier halogens, which are thought to be almost wholly lost from the subducting slab and released much earlier in the subduction process, due to their larger ionic radii and thus higher incompatibility in mineral phases (Ito et al., 1983; Straub and Layne, 2003).

The analysis of whole rock igneous samples from the altered oceanic crust has recently been carried out by Chavrit et al. (2016) in order to constrain the halogen content of the oceanic crust and determine the halogen budget available for subduction. Pagé et al. (2016) have also shown that hydrous minerals including Na-amphibole, phengite and lawsonite in moderate pressure blueschists from a cold subduction zone — the Tavşanlı ophiolite of NW Turkey — contain up to 900 ppm F, 100 ppm Cl, 500 ppb Br and 1400 ppb I. Kendrick et al. (2018) showed that one garnet peridotite that reached eclogite facies conditions retained appreciable quantities of Cl, Br and I. However, there remains a paucity of data for subduction zone minerals and lithologies that have reached eclogite facies conditions in a warm subduction zone series of lithologies. This study provides a systematic investigation of halogen contents and distributions in eclogite facies, ophiolitic lithologies, using chemical and imaging techniques to measure and map halogen concentrations and distributions in high-pressure hydrous and anhydrous minerals from the Western and Central Alps.

2. GEOLOGICAL SETTING

2.1. Geological overview of the Alps

The massifs of the Western and Central Alps comprise part of the Alpine orogenic belt — an archetypal example of a collisional belt — which formed during the Alpine orogeny that began in the late Cretaceous (Dal Piaz et al., 2003). The convergence involved the closure of the Jurassic Piemont–Ligurian Ocean (De Wever and Baumgartner, 1995) and the Late Jurassic–Early Cretaceous Valais Ocean (Stampfli et al., 1998), through southward subduction of the Eurasian plate beneath Adria, a portion of the African plate (Handy et al., 2010). The main collision and peak high-pressure metamorphism occurred at ~40 Ma (Amato et al., 1999), in the middle Eocene. The widespread occurrence of zoisite eclogite in the region (Pognante, 1991) suggests that the Alpine subduction zone was a warm subduction zone (Schmidt and Poli, 1998). The subduction of the distal European margin is recorded in the blueschist to eclogite facies units of the Penninic nappes (Dal Piaz et al., 2003).

The Penninic nappes are comprised of the former European continental margin, the Briançonnais microcontinent and the ophiolitic Piemont Zone (Dal Piaz et al., 2001). The two areas within the Penninic nappes considered in this study are the Piemont Zone and the Central Alps (denoted as PZ and CA respectively in Fig. 1).

2.2. The Western Alps (Piemont Zone)

Piemont Zone lithologies include ophiicarbonates and terrigenous metasediments mixed with metabasalts and ophiolitic bodies, together with antigorite serpentinites derived from mantle peridotite that have been intruded by discontinuous metagabbro bodies, which are overlain by pillow basalts, metacherts and marbles (Dal Piaz et al., 2003). The Piemont Zone underwent low thermal regime metamorphism during contraction, resulting in blueschist to eclogite facies units, with peak conditions of 2.7–2.9 GPa and 600–630 °C (Amato et al., 1999).

To the south of the Piemont Zone lies the Monviso ophiolite massif (Fig. 1, locality 1). The Monviso complex consists of multiple units of metabasalts and metagabbro lenses separated by shear zones, within a serpentinite matrix (Guillot et al., 2004). Within the complex, the Lago Superiore unit records the highest conditions experienced, with peak pressures and temperatures of 2.4–2.7 GPa and 550–

620 °C (Messiga et al., 1999; Angiboust et al., 2012). Within the metagabbros are cross-cutting high-pressure veins (Spandler et al., 2011), local occurrences of chrome-rich omphacite (smaragdite), and occurrences of Mg-chloritoid, indicating a syn-eclogitic volatile component, suggested to be formed during the breakdown of pre-eclogite volatile-bearing minerals (Messiga et al., 1999). The Monviso complex originated as part of the oceanic lithosphere of the Piemont basin (Lombardo et al., 1978).

The Orsiera-Rocciavré ophiolite (Fig. 1, locality 2) is equivalent to the Monviso massif. Within the Punta del Lago unit in Rocciavré, the metagabbros avoided plastic deformation and are cut by randomly oriented, centimetre scale eclogite veins (Philippot et al., 1998). The metagabbro body overlies large sections of serpentinite, with evidence of rodingitization between them (Bortolami and Dal Piaz, 1970), suggesting an ocean floor origin for the complex.

The St. Marcel valley (Fig. 1, locality 3) includes both oceanic and continental margins derived from the Piemont-Ligurian ocean and African crustal margin (Tartarotti et al., 2017). Metaophiolites in this region consist of hydrothermally altered metabasalts and metasediments, with rocks of uncommon mineralogy and chemistry that are enriched in Mn (by up to 39% wt% Mn_2O_3) and trace elements such as As, Bi, Co, Cu, Fe, Ni and Pb (Tumiati et al., 2010). The sediments overlying

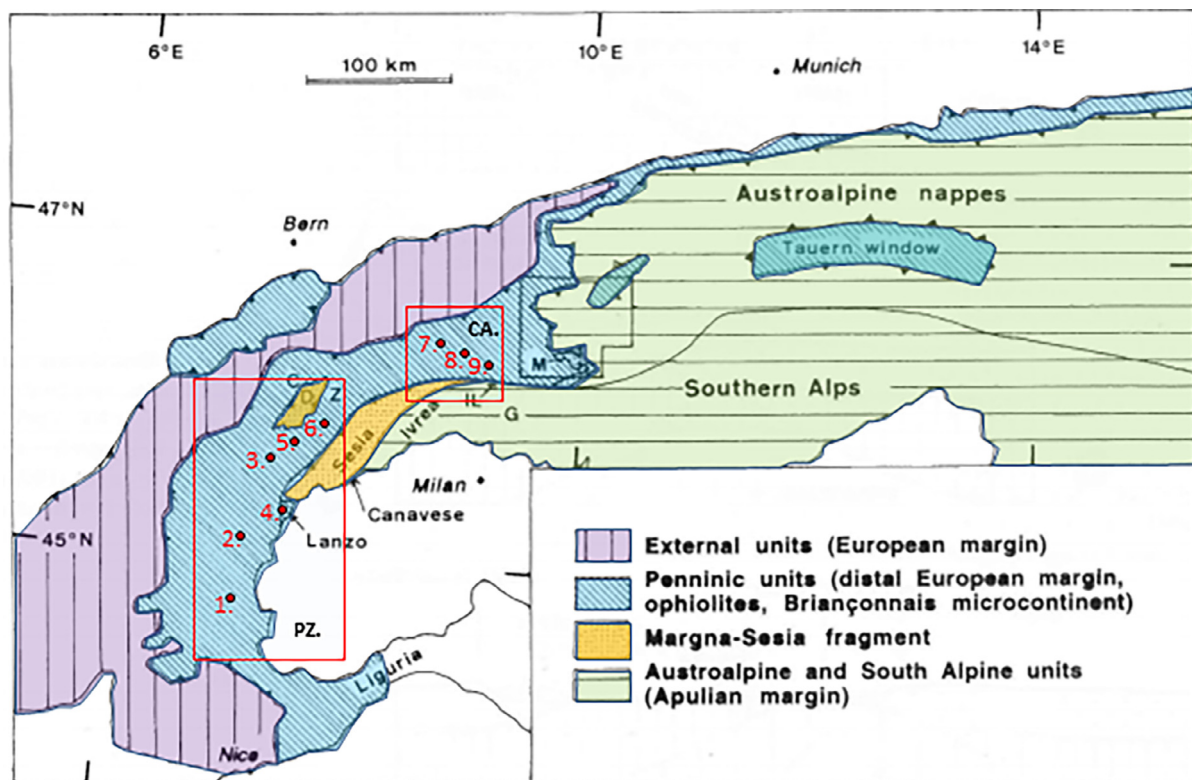


Fig. 1. Simplified geological map of the Western and Central Alps (after Froitzheim and Manatschal, 1996). Sample localities are marked with red circles and are numbered as described in Table 1. The two areas focused on in this study are enclosed in red boxes. Abbreviations correspond to: A – Adula nappe, C – Combin zone, CA – Central Alps, CL – Cima Lunga nappe, D – Dent Blanche nappe, G – Generoso basin, IL – Insubric line, M – Margna-Sella system, PZ – Piemont Zone, Z – Zermatt zone. (For interpretation of the references to colour in this figure legend, the reader is referred to the web version of this article.)

the metabasalts are interpreted to be the cover sequence of the oceanic lithosphere (Tartarotti et al., 1986). Peak conditions reached in this locality were 2.1 GPa and 550 °C (Martin et al., 2008).

The Lanzo massif (Fig. 1, locality 4) lies to the east of the Piemonte zone, south of the Sesia-Lanzo high-pressure terrane. Plagioclase lherzolite dominates at this locality, along with discontinuous bands of dunite and pyroxenite layers (Boudier and Nicolas, 1972; Boudier, 1976; Bodinier, 1988). The Lanzo Massif is thought to be a residual piece of upper mantle, after the extraction of T- to N-MORB type melts (Bodinier, 1988), which was then exhumed to the seafloor during the opening of the Piemonte-Ligurian ocean (Kaczmarek et al., 2008; Piccardo, 2010). To the north, the peridotite within the massif is surrounded by foliated serpentinites resulting from seafloor alteration and Alpine metamorphism (Kaczmarek et al., 2008). The dunites are interpreted as zones for preferential tapping of melt during MORB extraction, and the pyroxenites represent cumulate phases that rose to the surface in feeder dykes (Bodinier, 1988). Peak conditions reached by the Lanzo Massif during subduction were more than 2.0 GPa and ~585 °C (Pelletier and Müntener, 2006).

The Lago di Cignana region (Fig. 1, Locality 5) contains excellent exposures of the Zermatt-Saas ophiolite (ZSO), the protolith of which formed part of the Piemonte-Ligurian seafloor (Amato et al., 1999). The metaophiolite in this area consists of metalherzolites and pyroxenites, metagabbros, basalts and calcareous and siliceous sediments (Reinecke, 1998). Lago di Cignana is one of two Alpine regions that have occurrences of ultra-high-pressure (UHP) metamorphism, manifested as coesite-bearing rocks (van der Klaww et al., 1997). UHP rocks exist in small lenses only hundreds of metres in thickness, with ~2 km² areal extent, which sit above large quantities of serpentinite (van der Klaww et al., 1997; Reinecke, 1998; Amato et al., 1999). Overlying the eclogites are Mn-rich quartzites and metapelites containing coesite (Bearth, 1967). Previous P-T paths published for Lago di Cignana suggest peak conditions of 2.7–2.9 GPa and 600–630 °C (Reinecke, 1998).

The Allalin metagabbro (Fig. 1, Locality 6) is the largest and best preserved metagabbro body in the ZSO (Rubatto et al., 1998). The Allalin gabbro is a body of layered troctolite and olivine gabbro argued to represent underplating of mafic magmas at the base of the continental crust of the Apulian plate (Bucher and Grapes, 2009). During subduction, the gabbro was detached and incorporated into the underlying subducting slab. Little change occurred within the olivine and augite grains with increasing pressure, and the gabbro retained primary igneous, as well as metamorphic, eclogite assemblages (Meyer, 1983; Dale et al., 2007; Bucher and Grapes, 2009). With increasing pressures, fluid infiltration converted plagioclase within the gabbro to ultra-fine-grained zoisite + kyanite + jadeite + quartz, with a pervasive hydration event converting the assemblage to omphacite + zoisite + talc + chloritoid + garnet + kyanite + rutile at ~2.5 GPa and 610 °C (Bucher and Grapes, 2009).

2.3. The Central Alps (Cima di Gagnone)

In the Central Alps, the Adula-Cima Lunga unit contains metre to kilometre sized lenses of ultramafic bodies that correspond to the three massifs of Cima di Gagnone (Fig. 1, locality 7), Alpe Arami (Fig. 1, locality 8) and Monte Duria (Fig. 1, locality 9), which are exposed in a continuous and narrow horizon (Evans and Trommsdorff, 1978; Pfiffner and Trommsdorff, 1998; Scambelluri et al., 2014). The three massifs are located towards the southern end of the Adula-Cima Lunga unit, in what are the highest-grade regions of the nappe, with peak conditions of more than 2.5 GPa and 800 °C (Heinrich, 1982; Heinrich, 1986; Meyre et al., 1997; Meyre et al., 1999; Pfiffner, 1999). Within the ultramafic rocks of the Adula-Cima Lunga unit, the garnet peridotites and chlorite harzburgites are of particular interest. These rocks crystallised at higher grade conditions than other ultramafic rocks in the Western Alps (Evans and Trommsdorff, 1978).

At Cima di Gagnone, examples of garnet lherzolite are mostly confined to one ultramafic body — outcrop Mg160 — with other outcrops containing chlorite harzburgites (Scambelluri et al., 2014). The chlorite harzburgites are either prograde and stable at eclogite facies or formed during retrogression of the garnet peridotite (Trommsdorff, 1990). Interest in the Gagnone peridotites stems from the occurrences of rodingites within the chlorite harzburgites. The presence of rodingites indicates that the Gagnone peridotites were intruded by mafic phases and, therefore, represented part of the seafloor (Evans et al., 1979; Evans et al., 1981). Relics of clinohumite and olivine + ilmenite intergrowths (Evans et al., 1979) provide evidence that the Gagnone peridotites are secondary, i.e. they formed from the dehydration of serpentine. Evans and Trommsdorff (1978) report that no evidence of rodingites has been found at the related Alpe Arami and Monte Duria massifs. This suggests that they avoided intrusion by mafic phases and are, therefore, not as well constrained as being close to the seafloor as the Gagnone peridotites. However, olivine + ilmenite intergrowths within the Alpe Arami and Monte Duria assemblages (Möckel, 1969; Evans and Trommsdorff, 1978) may provide evidence of a similar origin. Nimis and Trommsdorff (2001) reported peak conditions at Cima di Gagnone of around 3.0 GPa and 740 °C.

The Alpe Arami massif consists of a small section (~1 km) of garnet lherzolite that is surrounded by kyanite-bearing eclogites (Green et al., 1997; Paquin and Altherr, 2000). Both show varying signs of lower pressure, hydrous alteration (Möckel, 1969). The exhumation history of the Alpe Arami peridotite is subject to debate. An ultra-deep, transition zone origin (300–600 km) was proposed by some authors, based on evidence such as FeTiO₃ rods in olivine, speculated to have originally exsolved as perovskite (Green et al., 1997), and former C2/c clinoenstatite lamellae in diopside (Bozhilov et al., 1999). This ultradeep origin has, however, been challenged by other authors. Risold et al. (2001) showed that the FeTiO₃ rods form after humite-type defects in olivine, and Trommsdorff et al. (2000) and Nimis and Trommsdorff (2001) suggest, instead,

peak conditions of 3.2 GPa and 840 °C. The Alpe Arami massif is believed to have an origin either as subducted sub-continental mantle (Trommsdorff et al., 2000) or mantle wedge (Brenker and Brey, 1997).

The Monte Duria massif is the final of the three garnet peridotite bodies within the Adula-Cima Lunga unit considered here. Fumasoli (1974) described the massif as consisting of 1–100 m sized lenses of peridotite which are embedded within biotite-plagioclase gneisses that are isoclinally folded. Hermann et al. (2006) argued that the Duria garnet peridotite originated in the mantle wedge above the European continental margin which was then assembled into country rock gneisses. Nimis and Trommsdorff (2001) suggested that peak metamorphic conditions in this massif were *ca.* 3.0 GPa and 830 °C.

3. SAMPLES

Rock samples were collected from the regions and localities discussed in Section 2. The major lithologies sampled, from which mineral separates were obtained, are described below. Sampling sites are shown in Fig. 1 and sample details, including minerals that were separated, are provided in Table 1. Mineral separation and preparation details are described in Section 4.1. Collected rock types include ultramafic peridotites and serpentinites, mafic metagabbros and metabasalts, hydrothermally altered metasediments and high-pressure veins cross-cutting eclogites. Rocks were collected based on the following criteria:

(1) high-pressure parageneses, manifested as eclogite or blueschist facies; (2) of demonstrably oceanic provenance, rather than continental; (3) minimal retrograde alteration; (4) presence of fluid inclusions or solid remnants of reacted fluid inclusions; and (5) presence of high-pressure hydrous minerals.

Peridotites were sampled in an attempt to find volatiles in existing or remnant fluid inclusions in subduction zone mantle rocks (e.g. Sumino et al., 2010). Olivine was separated as it is the main constituent of peridotite, and because some of the larger grains in the Cima di Gagnone samples contain relict fluid inclusions (Scambelluri et al., 1997; Kendrick et al., 2011; Scambelluri et al., 2015).

The serpentinite was sampled as serpentinites are claimed to be potentially important in returning water and other volatile elements to the deeper mantle (e.g. John et al., 2011; Kendrick et al., 2011; Debret et al., 2014; Kendrick et al., 2017). Serpentine contains large quantities of structurally bound H₂O (~12 wt%) and can remain stable up to pressures corresponding to ~200 km depth on a cold slab geotherm (Ulmer and Trommsdorff, 1995; Schmidt and Poli, 1998).

Metagabbros were sampled as the complexes they originate from — Monviso and Allalin — are believed to be ophiolitic in nature and thus represent the lower portions of subducted oceanic crust. Olivine and clinopyroxene were separated from samples DC25C and DC25D (Table 1) as these samples are only partially eclogitised and thus may retain some of their igneous volatile inventories. Omphacite was separated as it is a good example of the local

“smaragdite” variety of pyroxene (Cr-omphacite) found in the Alps region.

Metabasalts were included as during interaction with seawater, this unit of the oceanic crust can become appreciably hydrous in nature and thus volatile enriched, forming a variety of hydrous minerals such as epidote, lawsonite, glaucophane, talc, chlorite and chloritoid. Epidote was separated from DC30A (Table 1) as, being an epidosite, it is clearly of oceanic provenance and hydrothermal in nature. Glaucophane, chloritoid and talc were separated since they are high-pressure hydrous phases, and thus may retain volatiles to substantial depths.

Metasediments were sampled as the sedimentary cover sequence above the oceanic crust can become notably enriched in both F and I before subduction, due to the presence of organic and carbonate material. Given the Mn-enrichment within sediments from this region, they are good candidates for hydrothermally altered cover sequences. Quartz was separated because of its potential to trap volatiles in fluid inclusions during subduction, and because the texture of quartz grains within samples here is indicative of recrystallisation at high pressures. The fluid inclusions may be representative of volatiles from *ca.* 90 km depth within the subduction zone. Phengite was separated because of its hydrous nature, and the fact that it may remain stable to ~300 km depth (Schmidt and Poli, 1998).

Eclogite veins were sampled as they can potentially provide insight into the compositions of metamorphic fluids released during subduction of lower grade assemblages. Quartz was separated from the veins for the reasons previously stated, whilst glaucophane is, as mentioned, a high-pressure hydrous phase. Omphacite was separated from sample since it is a high-pressure phase that also contains fluid inclusions.

The following descriptions are based on optical microscopy analysis of each sample (Fig. 2).

3.1. Piemont Zone samples

3.1.1. Ultramafic rocks

Samples DC64B, DC67 and DC69 are coarse-grained ultramafic rocks collected from the Lanzo peridotite massif. Lanzo samples retain much of their igneous mineralogy and texture. They are essentially un-metamorphosed ultramafic rocks that show little evidence of reaction during subduction, and thus may retain the volatile signatures of their primary environment. DC64B is a websterite containing abundant exsolved pyroxene, minor olivine and plagioclase feldspar, with accessory Cr-spinel (Fig. 2a). DC67 is a harzburgite containing abundant medium to coarse-grained olivine and orthopyroxene, with minor clinopyroxene (Fig. 2b) and altered, Ca-rich plagioclase, with accessory amphibole and magnetite. Both pyroxenes in this sample contain exsolution lamellae, consistent with crystallisation at high temperatures (i.e. igneous settings). DC69 is a coarse-grained dunite, composed almost entirely of olivine, with accessory Cr-spinel.

Sample DC57 is an antigorite serpentinite collected from Lago di Cignana, and is composed mostly of fine-grained, mesh-textured antigorite. DC57 also contains occurrences

Table 1
Sample details.

Sample ID	Catalogue No. ^a	Location in Fig. 1	Lithology	Prepared fraction (mineral/mineral reflects mineral mixture)	Grid reference or lat/long
DC94B	21425	Monviso – Location 1 (PZ)	Metagabbro	Cr-omphacite	E 07° 05' 32" N 44° 41' 34"
DC97Di	21435	Monviso – Location 1 (PZ)	Omphacite vein in eclogite	Omphacite, Bulk rock	E 07° 05' 15" N 44° 41' 49"
RO85/127	20520	Rocciavré – Location 2 (PZ)	Vein within eclogite	Glaucophane, Quartz	~E 07° 10' 48" N 45° 02' 13"
DC46L	21328	St Marcel – Servette – Location 3 (PZ)	Metabasalt	Chloritoid, Talc	E 07° 27' 20" N 45° 42' 06"
DC48G	21430	St. Marcel - Fontillon – Location 3 (PZ)	Metabasalt	Chloritoid, Glaucophane	E 07° 27' 14" N 45° 42' 29"
DC58G	21362	St. Marcel - Praborina – Location 3 (PZ)	Metasediment	Quartz, Phengite	E 07° 27' 00" N 45° 40' 46"
DC58L	21366	St. Marcel - Praborina – Location 3 (PZ)	Metasediment	Quartz/Braunite	E 07° 27' 00" N 45° 40' 46"
DC64B	21380	Lanzo massif – location 4 (PZ)	Peridotite	Clinopyroxene, Orthopyroxene	E 07° 23' 37" N 45° 10' 36"
DC67	21385	Lanzo massif – location 4 (PZ)	Peridotite	Olivine, Orthopyroxene	E 07° 23' 42" N 45° 10' 36"
DC69	21386	Lanzo massif – location 4 (PZ)	Peridotite	Olivine	E 07° 23' 48" N 45° 10' 38"
DC50B	21343	Lago di Cignana – Location 5 (PZ)	Metasediment	Quartz	6120 0806
DC54C	21351	Lago di Cignana – Location 5 (PZ)	Glaucophane/quartz vein	Glaucophane, Quartz	6120 0806
DC54D	21352	Lago di Cignana – Location 5 (PZ)	Glaucophane/quartz vein	Quartz	6120 0806
DC57	21355	Lago di Cignana – Location 5 (PZ)	Serpentinite	Antigorite	6116 0806
DC25C	21274	Allalin – Location 6 (PZ)	Metagabbro	Clinopyroxene (Augite)	7191 1212
DC25D	21275	Allalin – Location 6 (PZ)	Metagabbro	Olivine	7191 1212
DC30A	21289	Täschalm – Location 6 (PZ)	Metabasalt	Epidote	6309 0984
DC21D (Mg160-1)	21258	Cima di Gagnone – Location 7 (CA)	Peridotite	Olivine	7078 1318
DC21G (Mg160-2)	21261	Cima di Gagnone – Location 7 (CA)	Peridotite	Olivine	7078 1318
DC21H (Mg160-3)	21262	Cima di Gagnone – Location 7 (CA)	Peridotite	Olivine	7078 1318
DC23A/B	21264/5	Alpe Arami – Location 8 (CA)	Peridotite	Olivine	7191 1212
DC19E	21241	Monte Duria – Location 9 (CA)	Peridotite	Olivine	7913 1314

^a Catalogue numbers of rock samples in the SEES geological collection, University of Manchester.

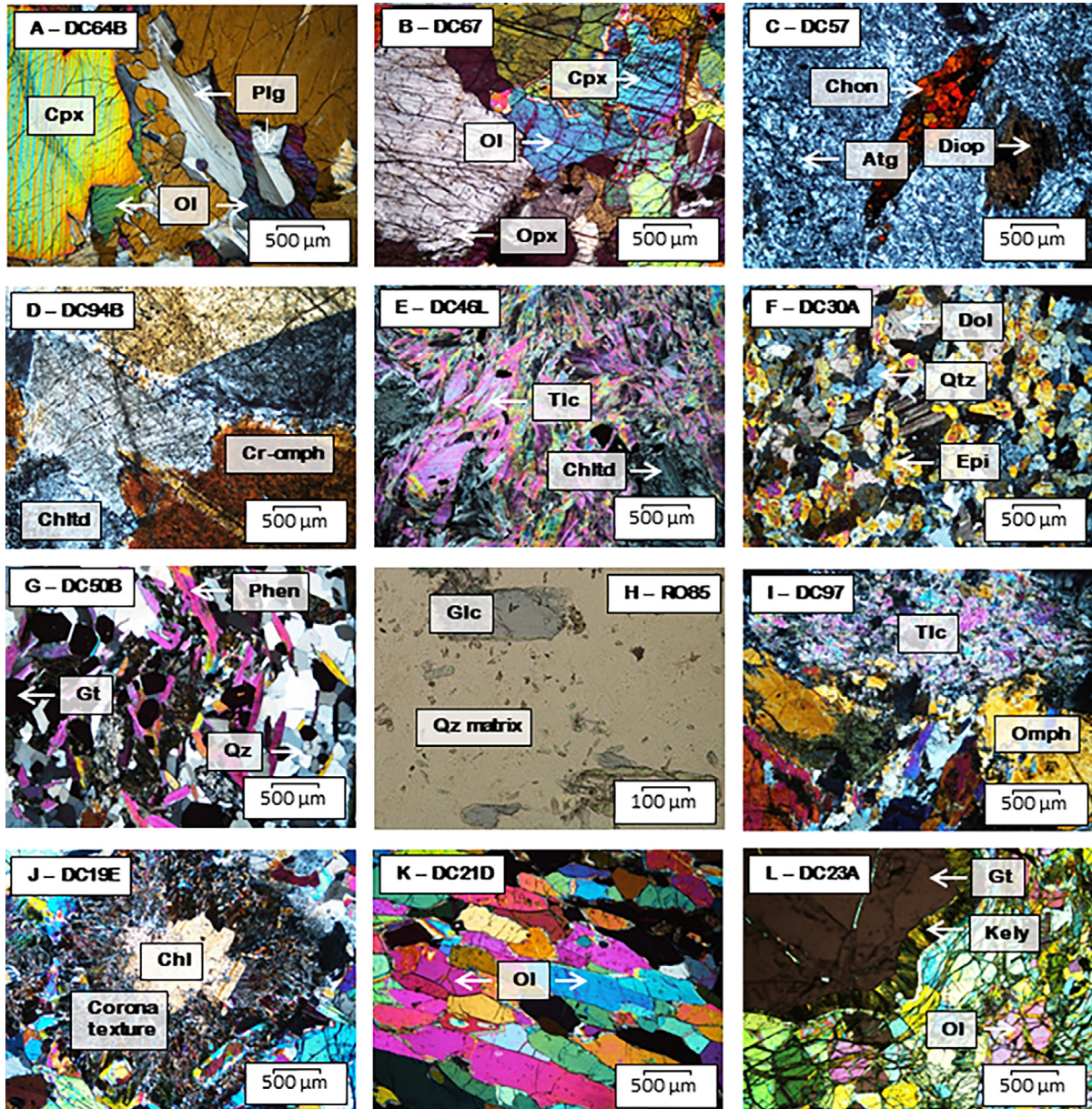


Fig. 2. Photomicrographs of samples from the Western and Central Alps in plane polarized light (PPL) and cross polarized light (XPL). (a) DC64B peridotite – XPL, (b) DC67 peridotite – XPL, (c) DC57 serpentinite – XPL, (d) DC94B metagabbro – XPL, (e) DC46L metabasalt – XPL, (f) DC30A metabasalt – XPL, (g) DC50B metasediment – XPL, (h) RO85/127 glaucophane + quartz vein – PPL, (i) DC97Di omphacite vein – XPL, (j) DC19E peridotite – XPL, (k) DC21D (Mg160-1) peridotite – XPL, and (l) DC23A peridotite – XPL. Atg = antigorite, Chl = chlorite, Chltd = chloritoid, Chon = chondrodite, Cpx = clinopyroxene, Diop = diopside, Dol = dolomite, Epi = epidote, Glc = glaucophane, Gt = garnet, Kely = kelyphite texture, Ol = olivine, Omph = omphacite, Opx = orthopyroxene, Phen = phengite, Plg = plagioclase, Qz = quartz, Tlc = talc.

of fine-grained, Ti-rich chondrodite and rare, fragmented, coarse-grained porphyroclasts of diopside, along with accessory magnetite (Fig. 2c).

3.1.2. Metagabbros

Samples DC25C, DC25D and DC94B are eclogite facies metagabbros collected from the Allalin (DC25C/D) and Monviso (DC94B) complexes. DC25C and DC25D are only partially eclogitised, retaining some igneous olivine

and augite. Plagioclase within the samples has mostly been converted into ultra-fine-grained zoisite + jadeite + kyanite + quartz. DC25C is a coarse olivine gabbro with abundant pyroxene, minor olivine, porphyroclasts of plagioclase and accessory amphibole and magnetite. DC25D is a coarse-troctolite containing abundant olivine, minor clinopyroxene and zoisite along with accessory chlorite and ilmenite. DC94B is coarse-grained and is mostly composed of omphacite and chloritoid (Fig. 2d), but also

contains minor medium-grained zoisite. As with DC25C and DC25D, the plagioclase in DC94B has been converted to ultra-fine-grained zoisite + jadeite + kyanite + quartz.

3.1.3. Metabasalts

Samples DC46L and DC48G are chloritoid-talc-rich metabasites collected from Servette and Fontillon, near St. Marcel. They are representative of a suite of eclogitised, former chlorite-rich, metasomatised mafic rocks (Martin et al., 2008). DC46L retains appreciable chlorite (~8% by volume), but is mostly composed of coarse-grained garnet, chloritoid and abundant fine-to-medium-grained talc (Fig. 2e), with minor quantities of rutile, pyrite, quartz, zoisite and apatite. DC48G is composed of abundant glaucophane, with smaller quantities of garnet and chloritoid, minor quantities of chlorite, talc and apatite, with accessory quartz, rutile, zoisite and paragonite. Sample DC30A is a garnet epidosite collected from Täschalm. It is composed of abundant fine-grained epidote and quartz, along with minor amounts of garnet and dolomite, with accessory paragonite, zoisite, apatite and pyrite (Fig. 2f).

3.1.4. Metasediments

Samples DC50B, DC58L and DC58G are metasediments collected from the Lago di Cignana and the Praborna manganese mine areas. DC50B is a garnet mica schist, in which phengite is surrounded by fine-grained quartz and garnet (Fig. 2g), with minor quantities of albite and accessory apatite and magnetite. DC58L is a manganese-bearing schist, composed of abundant, fine-grained piemontite (a Mn-rich epidote-group mineral), fine-grained braunite (a Mn-rich nesosilicate mineral) and coarse-grained phengite surrounded by quartz, with minor quantities of albite and accessory talc and apatite. DC58G is a Mn-rich mica schist and contains higher abundances of phengite relative to DC50B and DC58L, along with piemontite and accessory albite, braunite and apatite.

3.1.5. Eclogite veins

Samples DC54C, DC54D and RO85/127 are glaucophane + quartz veins collected from Lago di Cignana and Rocciavre. Sample RO85/127 is composed of medium-to-coarse-grained glaucophane set within a fine-grained quartz matrix (Fig. 2h), with accessory albite and apatite. The quartz matrix has a granoblastic texture, and individual grains have undulose extinction, suggesting plastic deformation affected these samples. Sample DC97Di is another eclogite vein sample, collected from Monviso, which is composed almost exclusively of omphacite, but also contains around 10% by volume of accessory phases such as albite, quartz, talc, chlorite and actinolite (Fig. 2i).

3.2. Central Alps samples

3.2.1. Ultramafic rocks

Samples DC19E, DC21D (Mg160-1), DC21G (Mg160-2), DC21H (Mg160-3), DC23A and DC23B are peridotites collected from the ultramafic bodies of Alpe Arami, Cima di Gagnone (Outcrop Mg160; Evans and Trommsdorff, 1978) and Monte Duria in the Central Alps region. The

peridotites generally have the mineralogy expected of garnet peridotite — mostly olivine, with variable proportions of orthopyroxene and Cr-diopside, but contain higher proportions of garnet than typical peridotite assemblages.

DC19E was sampled from Monte Duria and contains olivine that shows occasional fractures hosting magnetite. The most striking feature of this sample is the extensive replacement of garnet by chlorite pseudomorphs (Fig. 2j). DC19E also contains secondary amphibole associated with kelyphite reaction rims of garnet, along with ilmenite and Ni-sulfide. The chlorite pseudomorphs and kelyphite rims indicate overprinting of the eclogite facies assemblage, which likely involved the influx of a fluid phase at greenschist facies conditions.

DC21D (Mg160-1), DC21G (Mg160-2), DC21H (Mg160-3) are medium to coarse-grained samples from outcrop Mg160 of Cima di Gagnone. Samples DC21D (Mg160-1) and DC21G (Mg160-2) both show a distinct preferred orientation of olivine and pyroxene prisms (Fig. 2k), suggesting that plastic deformation during subduction has affected these two samples. Sample DC21H (Mg160-3) has a similar mineralogy to DC21G (Mg160-2) but lacks the preferred orientation and, unlike DC21D (Mg160-1) and DC21G (Mg160-2), garnet within this sample has mostly reacted to form kelyphite, with only rare, small porphyroclasts remaining. Outcrop Mg160 samples all contain small quantities of amphibole in association with kelyphite rims of garnet, which have also been observed in this outcrop in previous studies (Kendrick et al., 2018). Accessory phases within Mg160 samples include ilmenite, magnetite, rutile, chalcophyllite and Cr-spinel. The characteristics of the three samples from Cima di Gagnone, and the presence of garnet, precludes them from being chlorite harzburgites that are also common in this locality (Trommsdorff, 1990; Scambelluri et al., 2014). The features described here suggest that Mg160 garnet peridotites have mostly retained their prograde metamorphic assemblages, but that they show some evidence of having undergone variable extents of retrogression.

DC23A and DC23B both show slight alteration, with olivine grains containing abundant cracks hosting magnetite. The garnet grains within the two samples also show small kelyphite reaction rims (Fig. 2l), with associated amphibole, suggesting some lower grade overprinting affected these samples, but which was not as extensive as occurred in DC21H (Mg160-3). Accessory phases in these samples include ilmenite and Cr-spinel.

4. ANALYTICAL METHODS

Aliquots of separated mineral fractions (Table 1) were neutron irradiated to convert Cl, Br and I into noble gas isotopes of Ar, Kr and Xe respectively (Kendrick, 2012a; Ruzié-Hamilton et al., 2016), which were then measured in NI-NGMS analysis. Mineral grains were fused using a CO₂ laser to provide a bulk measurement of halogens located within the mineral structure and fluid inclusions, and olivine separates in peridotites were also subjected to *in vacuo* crushing, prior to furnace heating, to establish if halogens were hosted primarily by fluid inclusions or the

mineral lattice. Additionally, F, Cl and Br were also investigated by *in situ* analytical and spatial mapping using electron-probe micro analysis (EPMA) and time-of-flight secondary ion mass spectrometry (TOF-SIMS), to further investigate halogen distributions.

4.1. Sample selection and irradiation

Halogen analysis in this study was performed primarily on mineral separates, with one bulk rock analysis. The rationale behind analysing mineral separates is that bulk rock chemistry can be estimated by combining the individual mineral separate data from within a rock, while also providing information on halogen distributions at the mineralogical and fluid inclusion scale. Rock samples were crushed and sieved and ~0.5–2.0 mm mineral grains were hand-picked under a binocular microscope. Only mineral separates representative of peak eclogite facies that showed the least signs of alteration were chosen. The separates were then washed in acetone using an ultrasonic bath, rinsed with de-ionised water, and then re-examined under the binocular microscope for further purification. Approximately 50–70 mg sized aliquots of the samples were then packed in Al foil packets, placed into quartz tubes and sealed under vacuum for irradiation. The samples were irradiated on the 16th May 2012, for 24 h, at the high flux reactor RODEO facility, Petten, Netherlands, with constant rotation (see [Supplementary Table A.1. for irradiation details](#)). Irradiation produces noble gas proxies as follows: Cl = $^{38}\text{Ar}_{\text{Cl}}$, Br = $^{80}\text{Kr}_{\text{Br}}$, I = $^{128}\text{Xe}_{\text{I}}$, Ca = $^{37}\text{Ar}_{\text{Ca}}$, K = $^{39}\text{Ar}_{\text{K}}$, Ba = $^{131}\text{Xe}_{\text{Ba}}$ and U = $^{134}\text{Xe}_{\text{U}}$. Irradiation standards used were the Hb3gr hornblende ([Turner et al., 1971](#)), scapolite minerals BB1, SP2 and BB2 ([Kendrick, 2012a](#)) and pyroxene from the Shallowater aubrite meteorite ([Gilmour et al., 2006](#)). Within the quartz tubes, Hb3gr monitors were placed at the top, bottom and middle, scapolite at the bottom and top, and Shallowater in the middle. The procedure followed for conversion of noble gas isotopes to parent elements is described in [Kendrick, 2012a](#) and [Ruzié-Hamilton et al. \(2016\)](#).

4.2. Noble gas mass spectrometry

Noble gas isotopes of mineral separates and one bulk rock sample ([Table 1](#)) were released by crushing (olivine only) and then furnace heating, or CO₂ laser step heating. Noble gas isotope determinations were carried out at the University of Manchester using the MS1 and ThermoFisher ARGUS VI mass spectrometers ([Ruzié-Hamilton et al., 2016](#)). Irradiation standards, monitors and corrections for determining halogen abundances via NI-NGMS are described and discussed in [Ruzié-Hamilton et al. \(2016\)](#).

Following irradiation, the samples were removed from the quartz tube and Al foil wrapping, and up to 10 mg sized aliquots were individually loaded into 3 mm diameter holes drilled into an Al sample holder. Each Al holder was placed into the laser port of the mass spectrometer and baked at ~120 °C for 24 h, to remove any adsorbed noble gases and to achieve the required vacuum inside the line. Noble gases were then liberated from each sample by progressively

increasing the laser power output, until the sample was fused, allowing complete extraction of any noble gases present. Liberated noble gases were then exposed to one hot and two cold NP10 SAES getters for 4 min for purification, followed by trapping onto a liquid nitrogen cooled finger of activated charcoal for a total of 5 min. The laser port was then isolated to minimize the blank contribution and the cold finger was then heated to 70 °C to release the noble gases and allow equilibration within the extraction line, before introducing them into the mass spectrometer.

Noble gas isotopes were determined using either the ThermoFisher ARGUS VI multi-collector mass spectrometer, or the custom-built MS1 mass spectrometer. For the ARGUS VI, Ar isotopes were collected on five Faraday cups using multi-collection, Kr isotopes were collected in a single step on the H2, H1, AX and L1 Faraday cups and Xe isotopes were collected using peak switching on a compact discrete dynode (CDD) multiplier. After nine measurement cycles data were regressed to inlet time ($t = 0$). For the MS1 measurements all isotopes were measured by peak jumping using magnetic field switching with a Faraday cup (Ar isotopes) or channeltron multiplier (Kr and Xe isotopes). Data regression to time-zero followed the same protocol as used for data acquisition via the ARGUS VI mass spectrometer. Halogen determinations and ratios (Br/Cl and I/Cl) are reported at 1 σ level of uncertainty.

4.3. Time-of-flight secondary ion mass spectrometry (TOF-SIMS)

Halogen distributions and abundances within grains and at grain boundaries were mapped using TOF-SIMS with the IDLE 3 instrument ([Henkel et al. 2006](#)). The IDLE 3 instrument is equipped with a multi-channel plate detector, followed by a scintillator and a photomultiplier. A ~1 nA Au⁺ direct current beam focused to a spot size of ~1 μm was used to sputter away the carbon coat and clean the sample surface over selected areas ranging in size from 50 to 150 μm across. Following surface cleaning, high mass resolution ($m/\Delta m > \sim 3000$) negative and positive secondary ion mass spectra were acquired for 15–30 min using a pulsed Au⁺ primary beam (see details in [Joachim et al., 2015](#)). With such an analytical setup, only a few nanometres were sputtered away during analysis (e.g., [King et al. 2010](#)), and observed distributions thus correspond to those at the surface of the studied samples.

Abundances of F, Cl and, where possible Br, were calculated based on calibrations relating the F/O, Cl/O and Br/O secondary ion ratios measured using TOF-SIMS with the known F, Cl and Br abundances of well-established glass and scapolite reference materials (glasses ALV-519-4-1, GL-D30-1, GL-D52-5, NIST 610, NIST 612, and scapolite samples BB1 and BB2; [Kendrick, 2012a](#); [Clay et al., 2013](#); [Joachim et al., 2015](#); [Ruzié-Hamilton et al., 2016](#); [Marks et al., 2017](#)). The 95% confidence intervals associated with the slopes of these standard calibration lines were $\pm 14\%$ for F, $\pm 20\%$ for Cl and $\pm 71\%$ for Br. Varying chemical compositions and structures (crystal/amorphous) of analysed material can have small effects on relative sensitivity factors determined for secondary ion emission (e.g.

Shimizu and Hart, 1982). To counteract this possible matrix effect, the analysed areas were pre-sputtered for ~10–20 min before analysis, to amorphise the surface of crystalline materials, after which it has been shown that relative sensitivity factors obtained for silicate glass standards can be applied to crystalline silicate samples (Stephan, 2001; Stephan and Lyon, 2013). Finally, halogen signals were observed to increase progressively with time during analyses, considered to be due to re-deposition of these species from the vacuum between two primary beam pulses. Therefore, the F/O, Cl/O and Br/O ratios correspond to time-zero intercepts calculated from regressions of F/O, Cl/O and Br/O vs. time. Detection limits of 92 ± 73 ppm F, 307 ± 183 ppm Cl and 38 ± 55 ppm Br were determined (background \pm 3SD), based on repeated analyses of the volatile- and halogen-free San Carlos olivine. Data reduction was carried out as follows: (i) F, Cl and Br abundances were calculated from the measured F/O, Cl/O and Br/O ratios and the corresponding standard calibration lines; (ii) only analyses with abundances $>$ background + 3SD were retained; (iii) the measured background F, Cl and Br abundances were subtracted from the calculated F, Cl and Br abundances; (iv) uncertainties were first calculated by propagating internal errors associated with each analysis and the uncertainties on calibration slopes (e.g., uncertainty 1 (in ppm) = calculated concentration $\times \sqrt{[(\text{internal error in } \%)^2 + (\text{calibration error in } \%)^2]}$); (v) total uncertainties were then calculated by propagating uncertainty 1 and uncertainties on background abundances (e.g., total error (in ppm) = $\sqrt{[(\text{uncertainty 1 in ppm})^2 + (\text{background uncertainty in ppm})^2]}$). As a result, for analyses with halogen concentrations close to the measured halogen background levels, uncertainty on the background dominates the total uncertainty, whereas the uncertainties associated with standard calibration lines dominate for analyses with high halogen abundances. Uncertainties associated with TOF-SIMS halogen abundances are reported at the 3σ level.

4.4. Electron-probe micro analysis (EPMA)

Analysis of Si, Al, Fe, Ca, Na, Mg, K, Ti, Mn, Cr, Ni, P, F and Cl was carried out at with a Cameca SX100 electron microprobe, using wavelength dispersive spectrometry (WDS). Operating conditions were 15 kV accelerating voltage with a two-condition setup of 20 nA beam current for major elements and 100 nA beam current for trace elements. Counting was conducted on $K\alpha$ lines for all elements, with 20 s counting times for Si, Fe, Mg, Al, Ca, K, Na, Mn, Cr, Ni, P and Ti and 180 s for F and Cl. A PC0 diffracting crystal was used for the analysis of F to enhance both peak resolution and total counts. The increased resolution is important for resolving the Fe $L\alpha$ peak from the F $K\alpha$ peak to ensure that the measured F is not simply a shoulder of the Fe $L\alpha$ peak in Fe-rich phases. Interference from the Mg $K\alpha$ peak on the F $K\alpha$ peak was minimised through pulse height analysis settings. During standardisation and analysis, time-zero regression was performed for F, Cl, Na and K to account for any decrease in count rates with time due to element migration. Using this analytical setup, detection limits for F and Cl

were ~100 ppm and ~18 ppm, respectively. Quantification standards used were wollastonite (Ca, Si), corundum (Al), fayalite (Fe), jadeite (Na), periclase (Mg), K-feldspar (K), rutile (Ti), tephroite (Mn), Cr_2O_3 (Cr), NiO (Ni), apatite (P, F) and sodalite/halite (Cl). Analysis was performed in stoichiometric mode of the Cameca software, which automatically assigned O based on pre-defined valences of the elements of interest, and $\text{H}_2\text{O}/\text{CO}_2$ was assumed by difference. Mineral formulae were re-calculated using the following number of oxygen atoms: olivine 4(O); pyroxene 6(O); garnet 12(O); chlorite 14(O); feldspar 8(O); antigorite 7(O); epidote 12.5(O); quartz 2(O); dolomite 2(O); amphibole 23(O); talc 11(O); chloritoid 12(O); phengite 11(O); rutile 2(O); magnetite 1(O); ilmenite 3(O) and spinel 4(O). Uncertainties associated with EPMA data are reported at the 3σ level.

4.5. Bulk rock calculations

The bulk chemistry — both major element and halogen data — of samples was calculated from the major element and halogen data of individual major and accessory mineral phases analysed by EPMA, TOF-SIMS and NI-NGMS, along with their modal abundances in samples (Supplementary Material Table S4) calculated by point count analyses (min. 500 points per sample) using JMicroVision. Halogen abundances associated with retrograde phases (Supplementary Material Table S4) were not included in the bulk calculations. The caveat with these estimates is that for bulk Br and I concentrations, not every mineral phase present within every rock type was analysed via NI-NGMS. However, the separated minerals that were analysed by NI-NGMS comprised most of the respective sample (i.e. olivine in peridotite, antigorite in serpentinite etc.). Given this, remaining mineral phases that were not analysed via NI-NGMS would need to be extremely Br- and I-rich to shift calculated bulk estimates significantly (see supplementary data for example calculations). This is unlikely, as EPMA and TOF-SIMS analyses of minor phases did not reveal any unusually halogen-rich phases that could have influenced the bulk compositions.

5. RESULTS

Major element data, halogen concentrations and ratios in individual mineral separates, including retrograde phases, along with their modal abundances across all samples, are presented in Supplementary Material Tables S1–S10.

5.1. Bulk rock chemistry

Most ultramafic samples (Supplementary Material Tables S5 and S6) are calculated to contain <45 wt% SiO_2 , >40 wt% MgO and appreciable FeO (>7 wt%) (Supplementary Material Table S3). Sample DC64B has slightly higher SiO_2 and lower MgO and FeO contents, reflecting the higher abundances of clino- and orthopyroxene. Variation in CaO (0.2–8.5 wt%) and Al_2O_3 (0.2–6.5 wt%) contents is due to variable amounts of garnet, clinopyroxene

and spinel. All samples have low alkali content, with no more than 0.3 wt% Na₂O and 0.03 wt% K₂O, while the serpentinite contains up to ~0.3 wt% TiO₂, reflecting the presence of Ti-rich chondrodite.

Metagabbro samples (Supplementary Material Table S7) have up to 50 wt% SiO₂ and are less Mg-rich than ultramafic samples (9–22 wt% MgO; Supplementary Material Table S3). Instead, they are much richer in CaO and Al₂O₃, with 8–16 wt% and 12–20 wt%, respectively, reflecting the greater proportion of plagioclase feldspar. Metagabbro samples are also more alkali-rich than ultramafic samples, with up to 4 wt% Na₂O and ~0.15 wt% K₂O.

Metabasalt samples (Supplementary Material Table S8) have between 43–55 wt% SiO₂, >16 wt% Al₂O₃ and up to 3 wt% total alkalis. The higher CaO, SiO₂ and lower MgO contents of sample DC30A (Supplementary Material Table S3) is due to the higher abundances of epidote and quartz within this sample. The metabasalts are compositionally similar to tholeiitic basalts but have variable Na₂O content (0.02–2.65 wt%) due to the presence of glaucophane within some samples. Their low K₂O and TiO₂ contents (<0.10 wt% and <1.0 wt% respectively) suggests that they are N-MORB type basalts that have tapped a depleted upper mantle source.

Metasediment samples (Supplementary Material Table S9) are characterised by high SiO₂ content (~63–71 wt%; Supplementary Material Table S3), reflecting the high abundance of quartz within these samples. K₂O content is high relative to other lithologies (1.5–3.9 wt%) due to the presence of phengite. Metasediment samples also show variation in CaO (1.5–3.7 wt%) and Al₂O₃ (8–13 wt%) contents, due to variable amounts of garnet and/or piemontite within samples. Metasediment samples are highly enriched in Mn compared to other lithologies, with MnO ranging from 5 to 17 wt%.

5.2. Halogen abundances and ratios

Calculated bulk rock halogen concentrations and ratios are presented in Table 2. Fig. 3 shows bulk rock F, Cl, Br and I abundances together with previously published data on altered ocean crust (AOC) and blueschist samples (Philippot et al., 1998; Straub and Layne, 2003; Sano et al., 2008; Kendrick et al., 2015b; Chavrit et al., 2016; Pagé et al., 2016) and Fig. 4 shows plots of F vs. Cl, and Br and I vs. Cl in rock samples. In the following section, halogen ratios are reported as weight ratios.

Ultramafic samples contain 4.1–75.4 ppm Cl, 2.2–350.1 ppb Br and 0.6–40.2 ppb I (Fig. 3), with F below detection (~100 ppm) in all samples. Br/Cl ratios range from $(0.39–10.1) \times 10^{-3}$ and I/Cl ratios range from $(0.74–5.33) \times 10^{-4}$ (Table 2). Additionally, crushing analysis of olivine separates from samples DC67 and DC69 (Supplementary Material Table S2) released on average only 14% of the total halogen content.

Metagabbro samples contain below detection to 90 ppm F, 32.3–1316 ppm Cl, 8.1–3989 ppb Br and 0.3–471 ppb I (Fig. 3). Metagabbros have an F/Cl ratio of ~0.1, Br/Cl

ratios from $(0.25–3.03) \times 10^{-3}$ and I/Cl ratios from $(0.08–3.57) \times 10^{-4}$ (Table 2).

Metabasalt samples contain 188–445 ppm F, 3.2–23.8 ppm Cl, 3.8–8.2 ppb Br and 0.3–1.2 ppb I (Fig. 3). F/Cl ratios range from (18–21), Br/Cl ratios range from $(0.20–1.61) \times 10^{-3}$ and I/Cl ratios range from $(0.33–3.59) \times 10^{-4}$ (Table 2). The whole rock eclogite sample, DC97, analysed by NI-NGMS has similar halogen abundances (3.2 ppm Cl, 5.2 ppb Br and 1.2 ppb I) to bulk estimates of other metabasalts, suggesting that calculated bulk halogen abundances are realistic, and that no other halogen rich phases not analysed here are present in basaltic samples.

Metasediments contain 300–780 ppm F, 6.2–20 ppm Cl, 0.6–9.2 ppb Br and 0.03–0.3 ppb I (Fig. 3). F/Cl ratios range from (17–126), Br/Cl ratios from $(0.03–1.49) \times 10^{-3}$ and I/Cl ratios from $(0.02–0.43) \times 10^{-4}$ (Table 2). It is worth noting that phengite not analysed by NI-NGMS in samples DC58L and DC50B likely contains Br and I in similar abundances to DC58G. However, re-calculating estimates in Supplementary Material Table S4 for these two samples, based on similar Br and I abundances to sample DC58G, results in minimal shifting of bulk estimates, due to the much lower abundance of phengite in these samples.

Eclogite veins contain below detection to 87 ppm F, 6.3–98 ppm Cl, 7.8–204 ppb Br and 0.7–39 ppb I (Fig. 3). Veins have an F/Cl ratio of 7, Br/Cl ratios from $(0.67–3.16) \times 10^{-3}$ and I/Cl ratios from $(0.56–3.96) \times 10^{-4}$ (Table 2). Of the eclogite veins, the highest fluorine abundances are found in glaucophane + quartz veins, whereas the highest heavy halogen abundances are found in the omphacite vein (Supplementary Material Table S10).

The overall distribution of halogens between eclogite facies lithologies is varied (Fig. 3 and Table 2). Fluorine is concentrated within metabasalts and metasediments (~190–780 ppm) and decreases to below detection (~100 ppm) abundance with depth in the slab. Chlorine shows no significant trend with depth in the slab and is around 5–75 ppm across all lithologies, except for one metagabbro sample reaching up to ~1300 ppm. Br and I are, however, depleted within metasediments and metabasalts (~1–9 ppb Br and ~0.1–1 ppb I) and are more concentrated within ultramafic serpentinites and peridotites (~2–350 ppb Br and ~1–40 ppb) at depth within the slab.

5.3. Halogen distribution in mineral phases

The *in situ* abundances of F, Cl and Br mapped and analysed in individual mineral phases by TOF-SIMS and EPMA can be found in Supplementary Material Tables S1 and S5–S10. Fig. 5 shows TOF-SIMS-derived maps of F/O and Cl/O ratios in the omphacite separate of the halogen-rich metagabbro DC94B. The secondary ion maps show that within the interior of the mineral grain, F/O and Cl/O ratios are uniform and suggest that halogens are distributed within the crystal lattice, as opposed to primarily being hosted within fluid inclusions. At the spatial scale of TOF-SIMS analyses of samples — tens of microns across and a few nanometers depth — no localised areas with high halogen content, indicative of fluid inclusions exposed by

Table 2
Halogen content of Alpine samples.

	F (ppm)	Cl (ppm)	Br (ppb)	I (ppb)	F/Cl ratio	Br/Cl ($\times 10^{-3}$)	I/Cl ($\times 10^{-4}$)
Ultramafic rocks							
DC19E	<100	4.1 \pm 0.4	9.1 \pm 0.6	0.7 \pm 0.1	–	2.24(\pm 0.26)	1.78(\pm 0.30)
DC21D (Mg160-1)	<100	14.2 \pm 3.4	26.6 \pm 1.7	1.1 \pm 0.2	–	1.88(\pm 0.47)	0.74(\pm 0.22)
DC21G (Mg160-2)	<100	14.1 \pm 2.7	61.5 \pm 3.9	5.4 \pm 0.9	–	4.35(\pm 0.88)	3.82(\pm 0.45)
DC21H (Mg160-3)	<100	13.3 \pm 3.0	36.5 \pm 2.4	2.4 \pm 0.4	–	2.75(\pm 0.65)	1.82(\pm 0.51)
DC23A	<100	12.8 \pm 0.7	112.7 \pm 7.2	5.5 \pm 0.9	–	8.82(\pm 0.74)	4.34(\pm 0.75)
DC23B	<100	10.9 \pm 0.9	110.7 \pm 7.2	5.2 \pm 0.8	–	10.1(\pm 1.1)	4.73(\pm 0.83)
DC64B	<100	5.7 \pm 0.1	2.2 \pm 0.1	0.6 \pm 0.1	–	0.39(\pm 0.02)	1.06(\pm 0.18)
DC67	<90	75.4 \pm 3.5	350.1 \pm 32.1	40.2 \pm 5.9	–	4.65(\pm 0.48)	5.33(\pm 0.85)
DC69	<100	20.3 \pm 0.6	69.3 \pm 23.8	5.7 \pm 0.9	–	3.42(\pm 1.18)	2.82(\pm 0.45)
DC57	<100	20.6 \pm 1.5	36.8 \pm 2.3	3.9 \pm 0.7	–	1.79(\pm 0.18)	1.88(\pm 0.36)
Metagabbros							
DC25C	<100	32.3 \pm 5.6	8.1 \pm 0.5	1.0 \pm 0.2	–	0.25(\pm 0.05)	0.32(\pm 0.08)
DC25D	<100	41.5 \pm 5.7	120.8 \pm 8.1	0.3 \pm 0.1	–	2.91(\pm 0.45)	0.08(\pm 0.03)
DC94B	90.1 \pm 36.1	1316.4 \pm 28.5	3988.8 \pm 249.8	470.5 \pm 76.5	6.84 $\times 10^{-2}$ (\pm 0.03)	3.03(\pm 0.20)	3.57(\pm 0.59)
Metabasalts							
DC30A	188.0 \pm 19.0	9.0 \pm 1.6	3.8 \pm 0.2	0.4 \pm 0.1	21(\pm 4.3)	0.43(\pm 0.08)	0.44(\pm 0.14)
DC46L	391.5 \pm 48.1	21.5 \pm 5.3	8.2 \pm 0.4	0.7 \pm 0.1	18(\pm 4.9)	0.38(\pm 0.10)	0.33(\pm 0.09)
DC48G	444.7 \pm 54.2	23.8 \pm 2.5	4.8 \pm 0.3	0.3 \pm 0.1	19(\pm 3.1)	0.20(\pm 0.04)	0.13(\pm 0.06)
DC97	N/A	3.2 \pm 0.1	5.2 \pm 0.3	1.2 \pm 0.2	–	1.61(\pm 0.11)	3.59(\pm 0.61)
Metasediments							
DC50B	494.8 \pm 36.4	20.0 \pm 5.1	0.6 \pm 0.1	0.03 \pm 0.01	25(\pm 6.6)	0.03(\pm 0.01)	0.02(\pm 0.01)
DC58G	779.5 \pm 85.9	6.2 \pm 0.1	9.2 \pm 1.2	0.3 \pm 0.1	126(\pm 14)	1.49(\pm 0.20)	0.43(\pm 0.14)
DC58L	302.3 \pm 31.5	17.9 \pm 3.9	1.1 \pm 0.1	0.1 \pm 0.01	17(\pm 4.1)	0.06(\pm 0.01)	0.03(\pm 0.01)
Eclogite veins							
RO85/127	86.9 \pm 21.7	11.7 \pm 0.5	7.8 \pm 0.4	0.7 \pm 0.1	7(\pm 1.8)	0.67(\pm 0.05)	0.56(\pm 0.08)
DC54C	N/A	14.2 \pm 0.2	29.6 \pm 1.6	1.0 \pm 0.1	–	2.09(\pm 0.12)	0.67(\pm 0.07)
DC54D	N/A	6.3 \pm 0.1	19.9 \pm 1.2	1.3 \pm 0.2	–	3.16(\pm 0.19)	1.98(\pm 0.10)
DC97	<100	97.8 \pm 1.8	203.9 \pm 12.6	38.7 \pm 6.4	–	2.08(\pm 0.13)	3.96(\pm 0.66)

the ion beam, were encountered. This of course does not preclude the existence of fluid inclusions in other areas that were not mapped, or below the depth of TOF-SIMS analysis in mapped samples.

To further assess the distribution of halogens in samples, a comparison between *in situ* and bulk analytical techniques is presented in Fig. A.1 of the supplementary material. Fig. A.1 shows that Cl concentrations in a common set of mineral phases measured by TOF-SIMS and EPMA are comparable to those measured by NI-NGMS. This comparison is consistent with TOF-SIMS secondary ion maps in suggesting that halogens measured in this study are primarily located within the crystal lattices of mineral phases.

6. DISCUSSION

6.1. Fluid inclusion vs. lattice-bound halogens

TOF-SIMS secondary ion maps of F/O and Cl/O ratios show that halogens are distributed uniformly throughout the omphacite separate in DC94B at the scale of analysis ($\sim 100 \times 100 \mu\text{m}$; Fig. 5). Given that only relatively small areas of mineral grains were mapped during a single spot analysis, and that these may not be representative, repeat maps across other grains within the same sample were carried out, and these also showed uniform halogen distribu-

tions. Uniform halogen distributions observed via TOF-SIMS, coupled with *in situ* abundances by TOF-SIMS and EPMA that match those measured by NI-NGMS (Fig. A.1), both suggest that the concentrations of halogens measured in this study are primarily bound within the structure of the mineral. This is consistent with the results of crushing followed by heating experiments performed on olivine separates. Crushing followed by heating can discriminate between halogen signatures in fluid inclusions and mineral lattices respectively (Chavrit et al., 2016). Crushing of olivine separates showed that fluid inclusion halogens represent a minor fraction of the total halogens — < 15% — with little difference in Br/Cl and I/Cl ratios between the halogens released by both techniques (Supplementary Material Table S2).

It is further useful to compare the Cl concentrations measured in samples here to those of experimentally synthesised nominally anhydrous minerals (NAMs), to determine if Cl abundances measured in this study are within experimentally constrained solubility values and are, therefore, able to be accommodated in the mineral structure. Experimental studies have shown that Cl is highly incompatible in synthesised NAMs, and Cl solubility at conditions between 2.0–2.6 GPa and 900–1300 °C can range from 2–133 ppm Cl in olivine and 3–119 ppm Cl in orthopyroxene, with temperature having no significant effect on solubility (Bernini

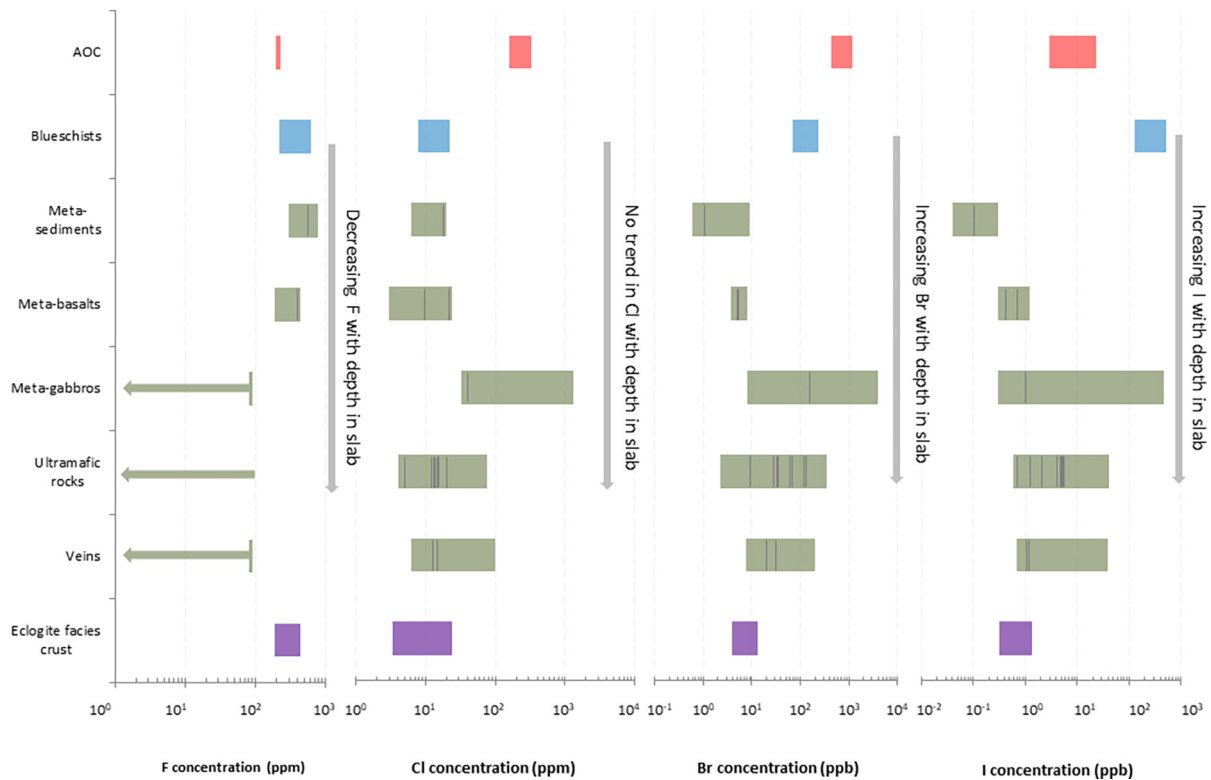


Fig. 3. Summary diagram of estimated bulk rock halogen abundances in Alpine samples compared with previously published AOC and blueschist data – estimates of halogen content within eclogite facies crust (see text and [supplementary information for calculations](#)) are also included. F and Cl are reported in ppm, Br and I in ppb. Vertical lines within boxes represent data points that range between minimum and maximum concentrations. AOC data are from [Philippot et al. \(1998\)](#), [Straub and Layne \(2003\)](#), [Sano et al. \(2008\)](#), [Kendrick et al. \(2015b\)](#) and [Chavrit et al. \(2016\)](#) and blueschist data are from [Pagé et al. \(2016\)](#).

[et al., 2013](#); [Fabbrizio et al., 2013](#)). Therefore, the concentrations of Cl measured here in olivine and pyroxene separates (up to ~100 ppm; [Supplementary Material Table S2](#)) are not unusually high, and thus can be accommodated within the crystal lattice.

Given the increasingly incompatible behaviour from Cl to I within solid phases, and the paucity of experimental data on the maximum solubility of Br and I in mineral phases, the Cl distributions and concentrations mapped and measured by TOF-SIMS ([Fig. 5](#)) and EPMA ([Supplementary Material Tables S5–S10](#)) may also be used as proxies for Br and I distributions. For Br in the case of the omphacite in sample DC94B, this assumption appears true, as Br was quantified *in situ* by TOF-SIMS ([Supplementary Material Table S1](#)). Uniform distributions of Cl observed and quantified *in situ*, together with the results of crushing of olivine separates, therefore, suggest that Br and I abundances measured in samples are also likely to be primarily within the crystal lattice.

Overall, all evidence suggests that the halogen concentrations measured in this study are hosted predominantly within the mineral lattice. Thus, they place constraints on the inventory of halogens that potentially can be returned to the deeper mantle via subduction.

6.2. Halogen abundances in eclogite facies rocks

Based on the calculated peak metamorphic conditions in the region ([Brenker and Brey, 1997](#); [Amato et al., 1999](#); [Paquin and Altherr, 2000](#); [Nimis and Trommsdorff, 2001](#)), halogen abundances in this study are taken to represent halogens from depths of >80 km within the subduction zone, since samples: (i) show prograde parageneses stable at high-pressure; (ii) are of oceanic provenance; and (iii) show minimal retrogression. The presence of a wide variety of hydrous minerals is consistent with seafloor alteration of the crust prior to its subduction. However, the Cl contents of eclogites in this study (3–24 ppm; [Table 2](#)) are lower than that of the AOC (~150–350 ppm; [Philippot et al., 1998](#); [Sano et al., 2008](#); [Chavrit et al., 2016](#)) and are similar to Tavşanlı blueschists (8–22 ppm; [Pagé et al., 2016](#)) ([Fig. 3](#)). The Cl contents of metasediments (<20 ppm) and ultramafic rocks (<75 ppm) in this study are also much lower than marine sediments (640 ppm; [Straub and Layne, 2003](#)) and oceanic serpentinites (677–1700 ppm; [Kendrick et al., 2013](#); [Chavrit et al., 2016](#)), indicating that the majority of Cl has been expelled from the slab before reaching eclogite facies conditions ([Fig. 3](#)).

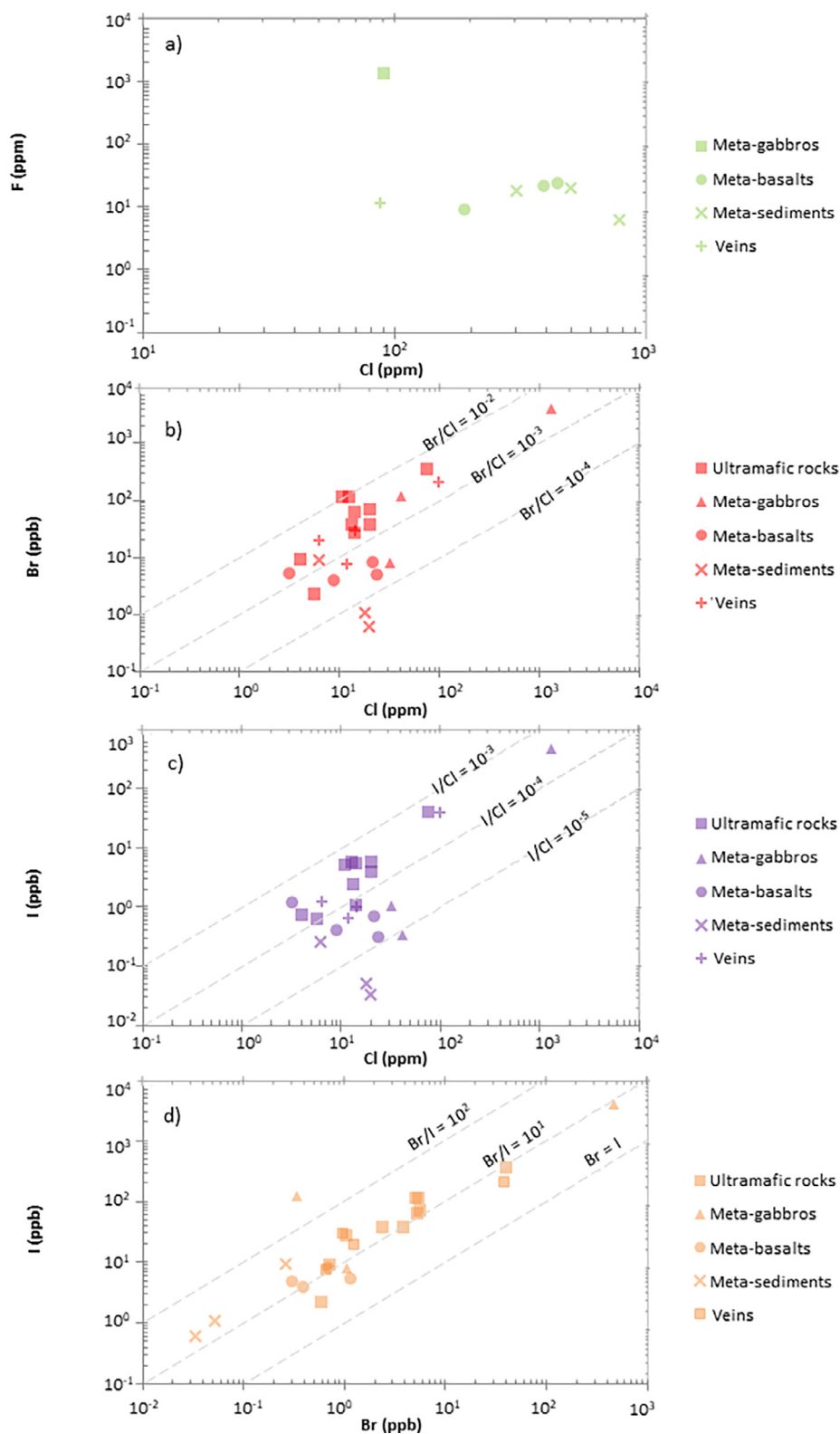


Fig. 4. Plots of (a) F vs. Cl, (b) Br vs. Cl, (c) I vs. Cl and (d) I vs. Br abundances in Alpine samples.

Relatively few studies have been carried out on the concentrations of Br and I in the AOC. Amphibole is postulated to be the major halogen hosting phase within the

AOC (Ito et al., 1983). Kendrick et al. (2015b) used secondary amphiboles in samples of oceanic metagabbros and amphibolites as an approximation for the Br

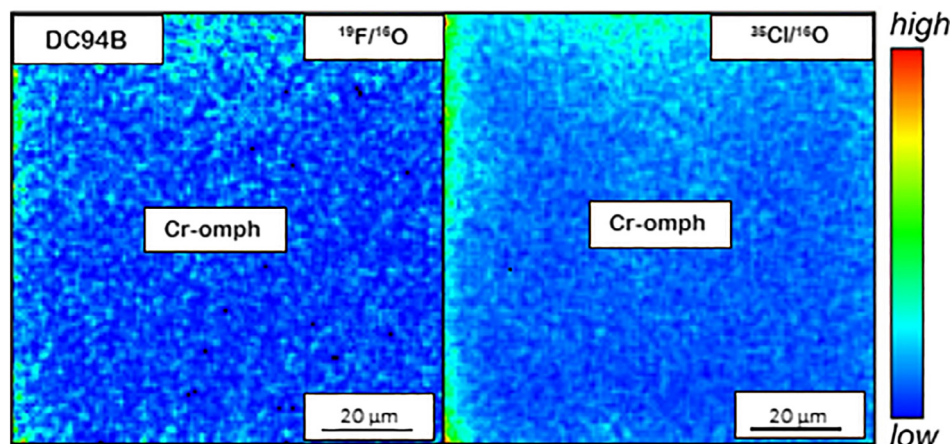


Fig. 5. Secondary ion maps of $^{19}\text{F}/^{16}\text{O}$ (left) and $^{35}\text{Cl}/^{16}\text{O}$ (right) ratios across Cr-omphacite in metagabbro sample DC94B.

(avg. 1199 ppb) and I (avg. 23 ppb) content of AOC material. Chavrit et al. (2016) analysed the Br and I content of 28 whole-rock igneous samples of altered oceanic crust from 5 ODP sites and obtained Br and I concentrations of 44–2500 ppb Br and 0.4–250 ppb I, with an average of 435 ppb Br and 3 ppb I. The Br and I concentrations within eclogites in this study (4–8 ppb Br and 0.3–1.2 ppb I) are up to two orders of magnitude lower for Br, and one order of magnitude lower for I, than that of the AOC (Fig. 3). The Tavşanlı blueschists (Pagé et al., 2016) also contain one order of magnitude more Br and two orders of magnitude more I than Alpine eclogites (Fig. 3). The Br and I concentrations of Alpine metasediments (<10 ppb and <1 ppb, respectively) and ultramafic rocks (<350 ppb and <40 ppb, respectively) in this study are more than two orders of magnitude lower than marine shales (14.8 ppm Br and 1.8–2.3 ppm I; Fuge, 1988; Muramatsu and Wedepohl, 1998; Chai and Muramatsu, 2007) and more than an order of magnitude lower than oceanic serpentinites (3178–6800 ppb Br and 580–751 ppb I; Kendrick et al., 2013; Chavrit et al., 2016). Similarly low concentrations of heavy halogens as in the Alpine ultramafics here have been measured in abyssal serpentinites subducted to blueschist facies (Pagé and Hattori, 2017). These abundances suggest that like Cl, Br and I are also extensively lost from the slab prior to, or during eclogite facies metamorphism.

Eclogites in this study show a similar range in F abundances (190–440 ppm) to AOC (~216 ppm F; Straub and Layne, 2003) and Tavşanlı blueschists (222–616 ppm; Pagé et al., 2016), suggesting that F may be retained to substantial depths during the subduction of basaltic crust. Alpine metasediments here have F concentrations (300–780 ppm) approaching that of oceanic sediments (611–740 ppm F; Fuge, 1988; Straub and Layne, 2003). Pelagic sediments and clays are reported to contain high concentrations of both I and F (Li, 1982; Muramatsu et al., 2007). These have been inferred to explain high concentrations of F in subducted blueschist material, through their interaction with circulating fluids that penetrate the oceanic crust during seafloor alteration and/or extensional faulting at the outer rise (Pagé et al., 2016). The increased abundances of F

in metabasalts and metasediments, relative to metagabbros and peridotites, is likely related to the greater proportion of hydrous minerals such as phengite, talc and apatite within these lithologies. The retention of F relative to I is facilitated by the large contrast in their ionic radii. F has the smallest ionic radius at $\sim 1.34 \text{ \AA}$, which is comparable to that of the OH^- ion at $\sim 1.35 \text{ \AA}$. The ionic radius of I is 2.2 \AA and is too large to readily substitute for OH.

6.3. Halogens in eclogite facies minerals

In contrast to the depleted concentrations of heavy halogens among lithologies, relative to their protoliths, minerals within some samples show higher Cl abundances compared to the typical <20 ppm abundances found in most separates. For example, olivine and pyroxene from sample DC67, olivine from DC25D and Cr-omphacite from DC94B have more Cl than 20 ppm (Supplementary Material Table S2). The possible reasons for Cl enrichment in these samples are briefly considered in the context of their respective protoliths.

The olivine and pyroxene separates from the Lanzo harzburgite (DC67) are the most halogen-rich (up to 75 ppm Cl, 350 ppb Br and 40 ppb I) of all ultramafic separates analysed, by up to one order of magnitude. As Lanzo samples represent ultramafic rocks that underwent little reaction during subduction, it is likely that the higher halogen abundances in mineral separates from DC67 are representative of their primary environment. A reason for their high halogen abundances may lie in the complex history of the Lanzo massif. As the melt extracted from south of the body had T- to N-MORB compositions, while in the north the peridotite equilibrated with T-MORB (Bodinier, 1988), it is possible that the source mantle was slightly enriched, relative to the depleted upper mantle of which N-MORB melts are generated. Alternatively, Piccardo et al. (2007) propose that the Lanzo peridotite represents extended subcontinental lithospheric mantle that had its chemistry altered and, refertilised, by early melts with MORB-type affinity, during decompression melting of the upwelling asthenosphere.

The various geological histories of ultramafic samples in this study may, therefore, provide a record of volatile contents through multiple stages of subduction and metamorphism, with Lanzo samples (DC64, DC67 and DC69) reflecting pre-subduction, primary volatile signatures, the Lago di Cignana serpentinite (DC57) reflecting post-antigoritization volatile signatures and, finally, central Alps samples (DC19E, DC21D, DC21G, DC21H, DC23B and DC23A) reflecting final dehydration signatures after the formation of secondary olivines and pyroxenes. Whilst Cl, Br and I abundances within the antigorite serpentinite sample (DC57) are around an order of magnitude lower than those of Lanzo sample DC67, there is little difference between this serpentinite and the secondary peridotites of the Central Alps (Table 2). This suggests that upon the breakdown of antigorite serpentinite, Cl, Br and I can be retained within anhydrous garnet peridotite assemblages. Since heavy halogen contents of ultramafic samples are also generally higher than other lithologies studied (Fig. 3 and Supplementary Material Table S3), it implies that serpentinites and dehydrated garnet peridotites may exert a major control on the subduction of Cl, Br and I to beyond sub-arc depths. This is consistent with Kendrick et al. (2018), who also suggest that nominally anhydrous garnet peridotites can retain Cl, Br and I, and that antigorite serpentinites and related secondary peridotites are major sources for subducted volatiles to the mantle.

Olivine from the Allalin metagabbro (DC25C) also has higher Cl (~40 ppm) than the typical 20 ppm measured in other separates. As the metagabbro contains both primary igneous and metamorphic assemblages (Meyer, 1983; Dale et al., 2007; Bucher and Grapes, 2009), it is possible that some of the halogens in this sample, like DC67, are also of primary origin. However, Cl content in the olivine separate is around one order of magnitude less than in AOC, while its Br concentration is also lower than AOC (435 ppb; Chavrit et al., 2016) and the metagabbroic amphiboles representative of a Cl-rich alteration zone (1199 ppb; Kendrick et al., 2015b). The Br content of the olivine separate is also at the lowest limit of unaltered E-MORB Br content (260–3120 ppb; Kendrick et al., 2012b). The lower abundances of Cl and Br relative to AOC and MORB are consistent with some expulsion during prograde metamorphism, suggesting measured halogen abundances indeed reflect metamorphic concentrations. As the assemblage contains relict olivine and augite grains and has ultra-fine-grained zoisite + kyanite + jadeite + quartz, it suggests that this sample avoided the pervasive, syn-eclogitic hydration event that converted assemblages into omphacite + zoisite + talc + chloritoid + garnet + kyanite + rutile (Bucher and Grapes, 2009). Therefore, the Cl and Br within the olivine may reflect metamorphic concentrations prior to reaching eclogite facies and the associated hydration event.

The Cr-omphacite from the metagabbro body of Monviso (DC94B) displays extreme enrichment in the heavy halogens, relative to other samples, with thousands of ppm Cl and up to ppm levels of Br and I (Supplementary Material Table S2). Compared to other samples, halogen abundances in DC94B are unusual; however, as found in

other samples, TOF-SIMS and EPMA analyses reveal that halogen concentrations are in the mineral lattice (Fig. 5; Supplementary Material Tables S1 and S7). The Monviso metagabbro body shares a similar prograde metamorphic history to the Allalin gabbro, with a large-scale, syn-eclogitic hydration event occurring at high pressure and temperature, manifested in the crystallisation of OH-bearing Mg-chloritoid (Messiga et al., 1999). Along with Mg-chloritoid and Cr-omphacite, DC94B has ultra-fine-grained zoisite + kyanite + jadeite + quartz within its matrix, and the nature of the contacts between mineral phases is not defined by sharp boundaries that are indicative of chemical equilibrium (Fig. 2.d). The characteristics of sample DC94B suggest that it may have been effectively “frozen” shortly after the influx of fluid and, therefore, never reached chemical equilibrium at eclogite facies, in which case halogen concentrations may represent disequilibrium abundances. The Cr-omphacite has similar halogen ratios to other samples (Fig. 6 and Supplementary Material Table S2), suggesting a fluid of uniform heavy halogen composition fluxed through this sample. Interestingly, the high-pressure vein sample cross-cutting this metagabbro body (DC97) is also enriched in heavy halogens, and has similar Br/Cl and I/Cl ratios to the Cr-omphacite (Supplementary Material Table S2; S3), suggesting that the fluid fluxing through the Monviso body was rich in Cl, Br and I. The well-equilibrated, whole rock eclogite sample from Monviso (DC97; Table 2) does not display comparable enrichment in heavy halogens, and has concentrations similar to other samples in this study. Therefore, it is likely that sample DC94B is not representative of well-equilibrated, metamorphic halogen abundances.

6.4. Halogen concentrations and distributions at eclogite facies

Performing halogen analysis on a range of ophiolitic lithologies and estimating bulk rock halogen abundances allows a quantitative understanding into the spatial/depth distribution of halogens within eclogite facies crust. Based on a typical slab makeup of ~0.4 km sediments, ~6 km basaltic crust and ~0.3 km of ultramafic material (e.g. Straub and Layne, 2003; Barnes and Straub, 2010) and assuming that these proportions are retained at eclogite facies conditions, estimated halogen abundances within eclogite facies crust are: ~190–450 ppm F, 3–23 ppm Cl, 4–13 ppb Br and 0.3–1.3 ppb I, with halogen ratios F/Cl – (19–55), Br/Cl – $(5.5–11.2) \times 10^{-4}$ and I/Cl $(5.7–8.8) \times 10^{-5}$ (Fig. 3; Table 3). Eclogite facies Cl, Br and I abundances are more than one order of magnitude lower than those of the AOC (Fig. 3) and are similar to heavy halogen abundances in the mantle — 5 ± 2 ppm Cl, 13 ± 6 ppb Br and 0.3 ± 0.1 ppb I (Kendrick et al., 2018 and references therein). Fluorine, on the other hand, is much more readily retained within the slab, and perhaps even acquired, during or prior to subduction, with similar-to-higher F abundances at eclogite facies than in the AOC (Table 3; Fig. 3). Estimated heavy halogen concentrations in this study suggest that upon reaching eclogite facies conditions, the subducting slab has lost over 90% Cl, Br and I, relative to AOC

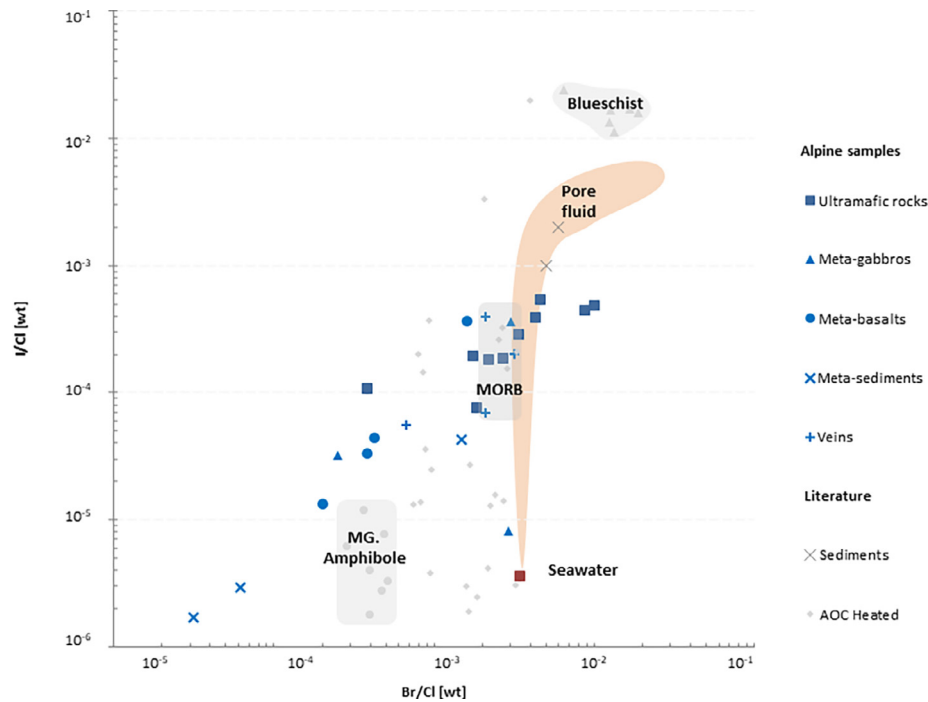


Fig. 6. I/Cl vs. Br/Cl ratios in Alpine samples compared to values reported in literature for subduction-related rocks and altered oceanic crust. Seawater and fields for sedimentary pore fluids and MORB are shown for reference. MORB field is from [Deruelle et al. \(1992\)](#), [Jambon et al. \(1995\)](#) and [Kendrick et al. \(2012b\)](#); Seawater is from [Li \(1982\)](#), AOC heated (heated \approx AOC whole rocks) are from [Chavrit et al. \(2016\)](#); Seafloor metagabbro amphibole separates (MG Amph.) are from [Kendrick et al. \(2015b\)](#); pore fluids are from [Kastner et al. \(1990\)](#), [Martin et al. \(1993\)](#), [Fehn et al. \(2006\)](#) and [Muramatsu et al. \(2007\)](#), and seafloor marine sediments are from [Muramatsu and Parr \(1985\)](#), [Suzuki and Hirai \(1992\)](#), [Yonezawa \(1996\)](#) and [Chai and Muramatsu \(2007\)](#).

abundances ([Chavrit et al., 2016](#)). These values are similar to the quantities of noble gases that are expelled during subduction (e.g. [Staudacher and Allègre, 1988](#)), and suggests that the process of subduction represents an efficient, but not complete, barrier to the subduction of volatile elements to the upper mantle. Indeed, this study shows that it may be possible for eclogite facies rocks to subduct tens of ppm Cl and ppb quantities of Br and I beyond the depths of the volcanic arc and into the upper mantle.

The high quantities of F calculated in the lithologies of the upper slab ([Table 2](#)) suggest that the major sinks that control the deeper subduction of fluorine are high-pressure hydrous phases such as phengite and talc, along with apatite, dependent on the abundance of P within the slab. The lack of fluorine within anhydrous minerals such as olivine and pyroxene suggests that incorporation mechanisms such as clumped F—OH defects ([Crepisson et al., 2014](#)), hydrated Si and Mg vacancies ([Shen et al., 2014](#)) and Ti-clinohumite lamellae ([Stalder and Ulmer, 2001](#)) do not play a significant role in the deeper transfer of F. Unlike F, however, the heavier halogens are depleted in the upper portions of the slab, implying that the same high-pressure hydrous phases are not significant carriers of heavy halogens to upper mantle depths. The low abundances of heavy halogens is consistent with increasing incompatibility with increasing ionic radii and, thus, lattice strain ([Blundy and Wood, 1994](#); [Blundy and Wood, 2003](#)). The higher abundances of Br and I within ultramafic material in this study,

relative to overlying mafic and sedimentary lithologies implies that, instead, ultramafic serpentinites and secondary olivine and pyroxene may be more important than more mafic, high-pressure hydrous phases in the deeper subduction of heavy halogens.

6.4.1. High-pressure veins

Given that halogens are incompatible and fluid mobile (e.g. [Ito et al., 1983](#); [Straub and Layne, 2003](#); [Bernini et al., 2013](#); [Fabbri et al., 2013](#); [Joachim et al., 2015](#)), high-pressure veins may offer insights into the nature of high-pressure fluids that were liberated during the breakdown of less stable assemblages during subduction.

The low F concentrations within vein samples ([Table 2](#)) suggest that either F has a propensity to remain within mineral phases during dehydration, or that the assemblage that broke down was already depleted in F. Our data imply that appreciable quantities of F remain within the slab at eclogite facies conditions, and [Pagé et al. \(2016\)](#) showed that blueschists also retain considerable F within lawsonite, Na-amphibole and phengite. Thus, vein-related samples with low F contents are consistent with previous suggestions that F is effectively retained within the subducting slab ([Straub and Layne, 2003](#)).

Abundances of Cl, Br and I within quartz separates derived from veins are generally higher than in sedimentary quartz ([Supplementary Material Table S2](#)). Thus, the halogens in vein-derived quartz are likely reflecting those hosted

Table 3
Estimated halogen content of Alpine eclogite facies crust.

	F (ppm)	Cl (ppm)	Br (ppb)	I (ppb)	F/Cl ratio	Br/Cl ratio ($\times 10^{-4}$)	I/Cl ratio ($\times 10^{-5}$)
Eclogite facies crust	190(± 18)-450(± 50)	3(± 1.5)-23(± 4.8)	4(± 0.2)-13(± 0.5)	0.3(± 0.1)-1.3(± 0.1)	19–55	5.5–11.2	5.7–8.8

in fluid inclusions. Given the small volume of fluid inclusions relative to quartz separates, it is likely that these fluid inclusions have relatively high abundances of heavy halogens. The high concentrations of Cl, Br and I within Alpine veins, and in sample DC97 in particular (Table 2), also supports halogen-rich eclogite facies fluids and heavy halogen mobility prior to or during eclogite facies metamorphism. High salinity fluids have also been observed in the Caledonides of Western Norway (Svensen et al., 2001). The halogen ratios of the Alpine veins fall in the same region as those of the metagabbros and the serpentinite (Fig. 6), suggesting that these lithologies were a potential source of fluids. This is consistent with suggestions by Spandler et al. (2011) that fluids within the Monviso complex originated from the serpentinites at the base of the gabbro.

6.5. Halogen behaviour during high-pressure subduction

The low concentrations of Cl, Br and I measured in Alpine samples imply that these elements are expelled from the subducting slab prior to reaching eclogite facies conditions. This is consistent with suggestions that Br and I have a high affinity for silicate melts and fluids (Bureau et al. 2010; Bureau et al. 2016), and that their large ionic radii inhibit their incorporation in mineral phases. Low concentrations of Cl are consistent with estimates by Jarrard (2003) that up to 75% of the Cl within rocks and pore fluids can be released from the accretionary wedge at <15 km depth. Similarly low Cl and Br abundances have been measured in metagabbros (<189 ppm Cl), blueschists (63–300 ppm Cl) and eclogites (28–60 ppm Cl) from Syros, Greece (Marschall et al., 2009), and in eclogites from western Norway (2–6 ppm Cl, 6–191 ppb Br; Svensen et al., 2001). Given that Alpine eclogites also show depletion in Cl, Br and I, relative to Tavşanlı blueschists (Pagé et al., 2016), which are themselves depleted when compared to AOC (Chavrit et al., 2016), it suggests that halogens are expelled in multiple stages throughout the subduction process. A first stage of devolatilisation involves major Cl loss prior to or during blueschist facies metamorphism (~0.6–1.5 GPa and 200–400 °C) in reactions such as antigorite + laumontite → lawsonite + quartz + H₂O and tremolite + chlorite + albite → glaucophane + epidote + H₂O. A second phase of halogen loss likely then occurs during the transition to eclogite facies metamorphism (>1.5 GPa and 400–500 °C) in reactions such as lawsonite → zoisite + grossular + cpx + qtz/coe + H₂O and glaucophane + paragonite → pyrope + jadeite + qtz + H₂O, which also expels I from the more hydrous phases in blueschist facies. These results are consistent with heavy halogens being less abundant in dehydrated lithologies, and consistent with the behaviour of H₂O and other volatile elements such as B and Li, in partitioning into fluid phases as subduction progresses (Scambelluri et al., 2004).

In contrast to the heavier halogens, our data suggest that F may be retained beyond the blueschist to eclogite transition, within the upper portions of the slab, in metabasaltic and metasedimentary material. Within the basaltic portion of the subducting slab, the minerals talc, chloritoid and apatite, which are stable at pressures above amphibole

breakdown (Schmidt and Poli, 1998), exert control on the return of F to sub-arc mantle depths. The low concentrations of F within epidote, paragonite, zoisite, chlorite and glaucophane suggest that these phases are not important carriers of F to deeper subduction depths. Within sedimentary material, the proportions of phengite and apatite control the amount of F available for subduction to sub-arc depths, as they may remain stable to substantial depths (Schmidt and Poli, 1998). The low Cl and high F abundances in basaltic material support previous claims by Straub and Layne (2003) that F is largely retained within the subducting slab, whilst Cl is almost totally recycled at the volcanic arc.

6.6. Halogen fractionation

Halogen ratios are independent of abundances, therefore, comparing halogen ratios of samples to those of major reservoirs such as the AOC may give insights into fractionation processes, and/or into identifying source contributions from the mantle and subducted components. The absence of a F–Cl correlation (Fig. 4a) suggests that the behaviour of F is de-coupled from heavy halogens, as alluded to in previous sections. This difference reflects the higher compatibility of F, relative to Cl, Br and I in silicate mineral structures, due to its more lithophile behaviour and similar ionic radius to the OH^- ion (Luth, 2003). No correlations between Cl and Br or I are evident (Fig. 4b, c), which suggests that Cl also behaves differently to Br and I during subduction. On the other hand, Br and I are well correlated (Fig. 4d) and, therefore, behave similarly at high pressure. The different behaviour of Cl may be explained by a preferential loss of Cl relative to Br and I at shallower depths of subduction, which is consistent with elevated F/Cl, Br/Cl and I/Cl ratios compared to AOC found both in this study (Fig. 6) and in Tavşanlı blueschists (Pagé et al., 2016). Given that there is little difference between the Cl abundances of the Tavşanlı blueschists (8–22 ppm; Pagé et al., 2016) and Alpine eclogites (3–24 ppm; Fig. 3), it suggests that most of the Cl loss during subduction occurs at depths shallower than blueschist facies conditions. Following major Cl loss at shallower depths, Br and I expulsion continues progressively to eclogite facies conditions, consistent with decreasing Br and I abundances from blueschist to eclogite samples (Fig. 3). This explains the lower Br/Cl and I/Cl ratios measured in Alpine eclogites, relative to those obtained for Tavşanlı blueschists (Pagé et al., 2016) (Fig. 6). In contrast to heavy halogen ratios, F/Cl ratios in eclogite samples (18–21; Table 2) are similar to those of Tavşanlı blueschists (25–74; Pagé et al., 2016), as F is retained in the slab to beyond sub-arc depths within hydrous minerals of the basaltic crust and sedimentary material.

7. CONCLUSIONS

Eclogite facies rocks from the Western and Central Alps contain low concentrations of Cl, Br and I, indicating major halogen loss occurs at shallower depths of subduction. Fluorine concentrations are variable depending on

lithology, and can be enriched within metabasalts and metasediments, relative to heavier halogens, suggesting that F is retained to sub-arc depths within the upper portions of the subducting slab. Conversely, Cl, Br and I are depleted within the upper portions of the slab relative to F, and are more concentrated in deeper ultramafic lithologies, highlighting their role in returning heavy halogens to sub-arc depths. Upon reaching eclogite facies conditions, the descending slab has lost over 90% Cl, Br and I. Bromine and iodine concentrations show positive correlation, suggesting that they exhibit similar behaviour at high pressure. A lack of correlation between any halogens other than Br and I suggests that F and Cl behave differently to Br and I during subduction. This is consistent with elevated F/Cl, Br/Cl and I/Cl ratios relative to AOC, suggesting Cl may be fractionated from F, Br and I during a preferential loss at depths shallower than blueschist facies conditions. The lack of correlation between F and Cl is likely due to the higher compatibility of F within silicate phases, related to the similar ionic radius of the F and OH^- ion. TOF-SIMS, EPMA and crushing vs. heating analyses suggest that halogens are distributed within the mineral lattice, as opposed to being concentrated in mineral or fluid inclusions. Halogen abundances within eclogite facies veins support the notion of F retention and Cl, Br and I mobility during subduction. Halogen concentrations in Alpine eclogites are lower than those measured in blueschist rocks, which in turn have lower concentrations than AOC samples, and can be explained by progressive halogen devolatilisation throughout the subduction process, consistent with the behaviour of H_2O . The halogen abundances determined in this study place constraints on the quantities that can be returned to the upper mantle, beyond sub-arc depths.

ACKNOWLEDGEMENTS

This manuscript forms part of the first author's PhD thesis, supported by the Natural Environment Research Council grant number NE/L002469/1, undertaken at the University of Manchester. Additional funding for this study from NERC grant NE/G01804/1 is also acknowledged. This grant was used to fund Déborah and Giles to collect the samples, make the thin sections and pay for the irradiation. We thank Steve Stockley for help preparing thin sections, Lorraine Ruzié for help with fine-tuning of the ARGUS VI mass spectrometer and Patricia Clay for providing halogen standards for use in TOF-SIMS analysis. We also thank two anonymous reviewers whose comments substantially improved the quality of this manuscript.

APPENDIX A. SUPPLEMENTARY MATERIAL

Supplementary data to this article can be found online at <https://doi.org/10.1016/j.gca.2018.09.024>.

REFERENCES

- Aiuppa A., Baker D. R. and Webster J. D. (2009) Halogens in volcanic systems. *Chem. Geol.* **263**(1–4), 1–18.
- Amato J., Johnson C., Baumgartner L. and Beard B. (1999) Rapid exhumation of the Zermatt-Saas ophiolite deduced from high-

- precision Sm–Nd and Rb–Sr geochronology. *Earth Planet. Sci. Lett.* **171**, 425–438.
- Angiboust S., Langdon R., Agard P., Waters D. J. and Chopin C. (2012) Eclogitization of the Monviso ophiolite (W Alps) and implications on subduction dynamics. *J. Metamorph. Geol.* **30**, 37–61.
- Barnes J. D. and Straub S. M. (2010) Chlorine stable isotope variations in Izu Bonin tephra: implications for serpentinite subduction. *Chem. Geol.* **272**, 62–74.
- Bearth P. (1967) Die Ophiolithe Zone von Zermatt. *Beitr. Geol. Karte Schweiz N.F.*, 1–132.
- Bernini D., Wiedenbeck M., Dolejs D. and Keppler H. (2013) Partitioning of halogens between mantle minerals and aqueous fluids: implications for the fluid flow regime in subduction zones. *Contrib. Mineral. Petrol.* **165**(1), 117–128.
- Blundy J. D. and Wood B. J. (1994) Prediction of crystal–melt partition coefficients from elastic moduli. *Nature* **372**, 452–454.
- Blundy J. D. and Wood B. J. (2003) Partitioning of trace elements between crystal and melts. *Earth Planet. Sci. Lett.* **210**, 383–397.
- Bodinier J. L. (1988) Geochemistry and petrogenesis of the Lanzo peridotite body, western Alps. *Tectonophysics* **149**, 67–88.
- Bortolami G. C. and Dal Piaz G. V. (1970) Il substrato cristallino dell'anfiteatro morenico di Rivoli-Avigliana (Prov. Torino.). *Mem. Soc. It. Sci. Nat.* **18**, 125–169.
- Boudier F. (1976) Le massif lherzolitique de Lanzo (Alpes piémontaises). Etude structurale et pétrologique. These d'Etat, Names, 175 pp.
- Boudier F. and Nicolas A. (1972) Fusion partielle gabbroïque dans la lherzolite de Lanzo (Alpes piémontaises). *Schweiz. Mineral. Petrogr. Mitt.* **52**, 39–56.
- Bozhilov K. N., Green H. W. and Dobrzhenetskaya L. (1999) Clinoenstatite in Alpe Arami peridotite: additional evidence of very high-pressure. *Science* **284**, 128–132.
- Brenker F. E. and Brey G. P. (1997) Reconstruction of the exhumation path of the Alpe Arami garnet–peridotite body from depths exceeding 160 km. *J. Metamorph. Geol.* **15**, 581–592.
- Bucher K. and Grapes R. (2009) The eclogite-facies Allalin Gabbro of the Zermatt–Saas ophiolite, Western Alps: a record of subduction zone hydration. *J. Petrol.* **50**, 1405–1442.
- Bureau H., Foy E., Raepsaet C., Somogyi A., Munsch P., Simon G. and Kubsky S. (2010) Bromine cycle in subduction zones through in situ Br monitoring in diamond anvil cells. *Geochim. Cosmochim. Acta* **74**(13), 3839–3850.
- Bureau H., Auzende A. L., Marocchi M., Raepsaet C., Munsch P., Testemale D., Mezouar M., Kubsky S., Carrière M., Ricolleau A. and Fiquet G. (2016) Modern and past volcanic degassing of iodine. *Geochim. Cosmochim. Acta* **173**, 114–125.
- Burgess R., Layzelle E., Turner G. and Harris J. W. (2002) Constraints on the age and halogen composition of mantle fluids in Siberian coated diamonds. *Earth Planet. Sci. Lett.* **197**, 193–203.
- Chai J. Y. and Muramatsu Y. (2007) Determination of bromine and iodine in twenty-three geochemical reference materials by ICP–MS. *Geostand. Geoanal. Res.* **31**, 143–150.
- Chavrit D., Burgess R., Sumino H., Teagle D., Droop G., Shimizu A. and Ballentine C. (2016) The contribution of the hydrothermal alteration of the ocean crust to the deep halogen and noble gas cycles. *Geochim. Cosmochim. Acta* **183**, 106–124.
- Clay P. L., O'Driscoll B., Gertisser H., Busemann H., Sherlock S. C. and Kelley S. P. (2013) Textural characterization, major and volatile element quantification and Ar–Ar systematics of spherulites in the Rocche Rosse obsidian flow, Lipari, Aeolian Islands: a temperature continuum model. *Contrib. Mineral. Petrol.* **165**, 373–395.
- Crepisson C., Blanchard M., Bureau H., Sanloup C., Withers A. C., Khodja H., Surble S., Raepsaet C., Beneut K., Leroy C., Giura P. and Balan E. (2014) Clumped fluoride–hydroxyl defects in forsterite: implications for the upper-mantle. *Earth Planet. Sci. Lett.* **390**, 287–295.
- Dale C. W., Gannoun A., Burton K. W., Argles T. W. and Parkinson I. J. (2007) Rhenium–osmium isotope and elemental behaviour during subduction of oceanic crust and the implications for mantle recycling. *Earth Planet. Sci. Lett.* **253**(1), 211–225.
- Dal Piaz G. V., Cortiana G., Del Moro A., Martin S., Pennacchioni G. and Tartarotti P. (2001) Tertiary age and paleostructural inferences of the eclogitic imprint in the Austroalpine outliers and zermatt-saas ophiolite, Western Alps. *Int. J. Earth Sci.* **90**(3), 668–684.
- Dal Piaz G. V., Bistacchi A. and Massironi M. (2003) Geological outline of the Alps. *Episodes* **26**(3), 175–180.
- Debret B., Koga K. T., Nicollet C., Andreani M. and Schwartz S. (2014) F, Cl and S input via serpentinite in subduction zones: implications for the nature of the fluid released at depth. *Terra Nova* **26**(2), 96–101.
- Deruelle B., Dreibus G. and Jambon A. (1992) Iodine abundances in oceanic basalts: implications for Earth dynamics. *Earth Planet. Sci. Lett.* **108**(4), 217–227.
- De Wever P. and Baumgartner P. O. (1995) Radiolarians from the base of the Supra-ophiolitic Schistes Lustres Formation in the Alps (Saint-Veran, France and Traversiera Massif, Italy). In *Middle Jurassic to Lower Cretaceous Radiolaria of Tethys: occurrences, systematics, biochronology*. Mem. Geol. (Lausanne) (eds. P. O. Baumgartner, L. O'Dogerty, S. Gorican, E. Urquhart, A. Pillevuit and P. De Wever). vol. 23, pp. 725–730.
- Evans B. W. and Trommsdorff V. (1978) Petrogenesis of garnet lherzolite, Cima di Gagnone, Lepontine Alps. *Earth Planet. Sci. Lett.* **40**, 333–348.
- Evans B. W., Trommsdorff V. and Richter W. (1979) Petrology of an eclogite–metaroddingite suite at Cima di Gagnone, Ticino, Switzerland. *Am. Mineral.* **64**, 15–31.
- Evans B. W., Trommsdorff V. and Goles G. G. (1981) Geochemistry of high-grade eclogites and metaroddingites from the Central Alps. *Contrib. Mineral. Petrol.* **76**, 301–311.
- Fabbri A., Stalder R., Hametner K. and Gunther D. (2013) Experimental chlorine partitioning between forsterite, enstatite and aqueous fluid at upper mantle conditions. *Geochim. Cosmochim. Acta* **121**, 684–700.
- Fehn U., Lu Z. and Tomaru H. (2006) Data report: 129I/I ratios and halogen concentrations in pore water of the Hydrate Ridge and their relevance for the origin of gas hydrates: a progress report. 24/32 In Proc. ODP, Sci. Results (eds. A. M. Tréhu, G. Bohrmann, M. E. Torres and F. S. Colwell). Ocean Drilling Program, College Station, TX, vol. 204, pp. 1–25. <https://doi.org/10.2973/odp.proc.sr.204.107.2006>.
- Froitzheim N. and Manatschal G. (1996) Kinematics of Jurassic rifting, mantle exhumation, and passive-margin formation in the Austroalpine and Penninic nappes (eastern Switzerland). *Bull. Geol. Soc. Am.* **108**, 1120–1133.
- Fuge R. (1988) Sources of halogens in the environment, influences on human and animal health. *Environ. Geochem. Health* **10**, 51–61.
- Fumasoli M. W. (1974) *Geologie des Gebietes nördlich und südlich der Jorio-Tonale-Linie im Westen von Gravedona (Como, Italia)* PhD Thesis. ETH, Zürich.
- Gilmour J. D., Pravdivtseva O. V., Busfield A. and Hohenberg C. M. (2006) The I–Xe chronometer and the early solar system. *Meteorit. Planet. Sci.* **41**, 19–31.

- Green H. W., Dobrzynetskaia L., Riggs E. A. and Jin Z. M. (1997) Alpe Arami: a peridotite massif from the mantle transition zone. *Tectonophysics* **279**, 1–21.
- Guillot S., Schwartz S., Hattori K., Auzende A. and Lardeaux J. (2004) The Monviso ophiolitic Massif (Western Alps), a section through a serpentinite subduction channel. In: (eds. M. Beltrando, G. Lister, J. Ganne and A. Boullier). *Evolution of the Western Alps: Insights from Metamorphism, Structural Geology, Tectonics and Geochronology*. Journal of The Virtual Explorer, vol. 16, p. 17.
- Handy M., Schmid S. M., Bousquet R., Kissling E. and Bernoulli D. (2010) Reconciling plate-tectonic reconstructions of Alpine Tethys with the geological-geophysical record of spreading and subduction in the Alps. *Earth-Sci. Rev.* **102**, 121–158.
- Heinrich C. A. (1982) Kyanite-eclogite to amphibolite facies evolution of hydrous mafic and pelitic rocks, Adula nappe, Central Alps. *Contrib. Mineral. Petrol.* **81**, 30–38.
- Heinrich C. A. (1986) Eclogite facies regional metamorphism of hydrous mafic rocks in the Central Alpine Adula nappe. *J. Petrol.* **27**, 123–154.
- Henkel T., Tizard J., Blagburn D. and Lyon I. C. (2006) Interstellar dust laser explorer (IDLE): a new instrument for submicron analyses of stardust—quantification of laser SNMS. *Appl. Surf. Sci.* **252**(19), 7117–7119.
- Hermann J., Rubatto D. and Trommsdorff V. (2006) Sub-solidus Oligocene zircon formation in garnet peridotite during fast decompression and fluid infiltration (Duria, Central Alps). *Mineral. Petrol.* **88**, 181–206.
- Hilton D. R., Fischer T. P. and Marty B. (2002) Noble gases and volatile recycling at subduction zones. *Rev. Mineral. Geochem.* **47**(1), 319–370.
- Holloway J. R. and Ford C. E. (1975) Fluid-absent melting of the fluoro-hydroxy amphibole pargasite to 35 kilobars. *Earth Planet. Sci. Lett.* **25**, 44–48.
- Ito E., Harris D. M. and Anderson A. T. (1983) Alteration of oceanic crust and geologic cycling of chlorine and water. *Geochim. Cosmochim. Acta* **47**(9), 1613–1624.
- Jambon A., Déruelle B., Dreibus G. and Pineau F. (1995) Chlorine and bromine abundance in MORB: the contrasting behaviour of the Mid-Atlantic Ridge and East Pacific Rise and implications for chlorine geodynamic cycle. *Chem. Geol.* **126**, 101–117.
- Jarrard R. D. (2003) Subduction fluxes of water, carbon dioxide, chlorine, and potassium. *Geochem. Geophys. Geosyst.* **4**(5), 8905.
- Joachim B., Pawley A., Lyon I. C., Marquardt K., Henkel T., Clay P. L., Ruzié L., Burgess R. and Ballentine C. J. (2015) Experimental partitioning of F and Cl between olivine, orthopyroxene and silicate melt at Earth's mantle conditions. *Chem. Geol.* **416**, 65–78.
- Joachim B., Stechern A., Ludwig T., Konzett J., Pawley A., Ruzié-Hamilton L., Clay P., Burgess R. and Ballentine C. (2017) Effect of water on the fluorine and chlorine partitioning behavior between olivine and silicate melt. *Contrib. Mineral. Petrol.* **172**(4), 15.
- John T., Layne G., Haase K. and Barnes J. (2010) Chlorine isotope evidence for crustal recycling into the Earth's mantle. *Earth Planet. Sci. Lett.* **298**(1–2), 175–182.
- John T., Scambelluri M., Frische M., Barnes J. and Bach W. (2011) Dehydration of subducting serpentinite: implications for halogen mobility in subduction zones and the deep halogen cycle. *Earth Planet. Sci. Lett.* **308**, 65–76.
- Kaczmarek M.-A., Müntener O. and Rubatto D. (2008) Trace element chemistry and U-Pb dating of zircons from oceanic gabbros and their relationship with whole rock composition (Lanzo, Italian Alps). *Contrib. Mineral. Petrol.* **155**, 295–312.
- Kastner M., Elderfield H., Martin J. B., Suess E., Kvenvolden K. A. and Garrison R. E. (1990) Diagenesis and interstitial-water chemistry at the Peruvian continental margin — major constituents and strontium isotopes. In: Proc. ODP, Sci. Results (eds. E. Suess, R. von Huene, et al.). Ocean Drilling Program, College Station, TX, vol. 112, pp. 413–440. <https://doi.org/10.2973/odp.proc.sr.112.144.1990>.
- Kendrick M., Scambelluri M., Honda M. and Phillips D. (2011) High abundances of noble gas and chlorine delivered to the mantle by serpentinite subduction. *Nat. Geosci.* **4**(11), 807–812.
- Kendrick M. (2012a) High precision Cl, Br and I determinations in mineral standards using the noble gas method. *Chem. Geol.* **292–293**, 116–126.
- Kendrick M., Kamenetsky V., Phillips D. and Honda M. (2012b) Halogen systematics (Cl, Br, I) in Mid-Ocean Ridge Basalts: a Macquarie Island case study. *Geochim. Cosmochim. Acta* **81**, 82–93.
- Kendrick M., Honda M., Pettke T., Scambelluri M., Phillips D. and Giuliani A. (2013) Subduction zone fluxes of halogens and noble gases in seafloor and forearc serpentinites. *Earth Planet. Sci. Lett.* **365**, 86–96.
- Kendrick M., Jackson M., Hauri E. and Phillips D. (2015a) The halogen (F, Cl, Br, I) and H₂O systematics of Samoan lavas: assimilated-seawater, EM2 and high-³He/⁴He components. *Earth Planet. Sci. Lett.* **410**, 197–209.
- Kendrick M., Honda M. and Vanko D. (2015b) Halogens and noble gases in Mathematician Ridge metagabbros, NE Pacific: implications for oceanic hydrothermal root zones and global volatile cycles. *Contrib. Mineral. Petrol.* **170**(5–6), 1–20.
- Kendrick M., Hémond C., Kamenetsky V., Danyushevsky L., Devey C., Rodemann T., Jackson M. and Perfit M. (2017) Seawater cycled throughout Earth's mantle in partially serpentinized lithosphere. *Nat. Geosci.* **10**, 222–228.
- Kendrick M. A., Scambelluri M., Hermann J. and Padrón-Navarta J. A. (2018) Halogens and noble gases in serpentinites and secondary peridotites: implications for seawater subduction and the origin of mantle neon. *Geochim. Cosmochim. Acta* **235**, 285–304.
- King A., Henkel T., Rost D. and Lyon I. C. (2010) Determination of relative sensitivity factors during secondary ion sputtering of silicate glasses by Au⁺, Au²⁺ and Au³⁺ ions. *Rapid Commun. Mass Spectrom.* **24**, 15.
- Kobayashi M., Sumino H., Nagao K., Ishimaru S., Arai S., Yoshikawa M., Kawamoto T., Kumagai Y., Kobayashi T., Burgess R. and Ballentine C. (2017) Slab-derived halogens and noble gases illuminate closed system processes controlling volatile element transport into the mantle wedge. *Earth Planet. Sci. Lett.* **457**, 106–116.
- Li Y. (1982) A brief discussion on the mean oceanic residence time of elements. *Geochim. Cosmochim. Acta* **46**(12), 2671–2675.
- Lombardo B., Nervo R., Compagnoni R., Messiga B., Kienast J. R., Mevel C., Fiora L., Piccardo G. B. and Lanza R. (1978) Osservazioni preliminari sulle ofioliti metamorfiche del Monviso (Alpi Occidentali). *Rendiconti della Società Italiana di Mineralogia e Petrologia*. **34**, 253–305.
- Luth R. W. (2003) Mantle volatiles—distributions and consequences. *Treat. Geochem.* **2**, 319–361.
- Lyubetskaya T. and Korenaga J. (2007) Chemical composition of Earth's primitive mantle and its variance: 1. Method and results. *J. Geophys. Res. Solid Earth* **112**(3), 1–21.
- Marks M. A. W., Kendrick M. A., Eby G. N., Zack T. and Wenzel T. (2017) The F, Cl, Br and I contents of reference glasses BHVO-2G, BIR-1G, BCR-2G, GSD-1G, GSE-1G, NIST SRM 610 and NIST SRM 612. *Geostand. Geoanal. Res.* **41**, 107–122.
- Marschall H. R., Altherr R., Gmeling K. and Kasztovszky Z. (2009) Lithium, boron and chlorine as tracers for metasoma-

- tism in high-pressure metamorphic rocks: a case study from Syros (Greece). *Mineral. Petrol.* **95**(3–4), 291–302.
- Martin J. B., Gieskes J. M., Torres M. and Kastner M. (1993) Bromine and iodine in Peru margin sediments and pore fluids: implications for fluid origins. *Geochim. Cosmochim. Acta* **57**, 4377–4389.
- Martin S., Rebay G., Kienast J. R. and Mével C. (2008) An eclogitised oceanic palaeo-hydrothermal field from the St. Marcel Valley (Italian Western Alps). *Ophioliti* **33**(1), 49–63.
- Messiga B., Kienast J. R., Rebay G., Riccardi M. P. and Tribuzio R. (1999) Cr-rich magnesiochloritoid eclogites from the Monviso ophiolites (Western Alps, Italy). *J. Metamorph. Geol.* **17**, 287–299.
- Meyer J. (1983) The development of the high-pressure metamorphism in the Allalin metagabbro (Switzerland). *Terra Cognita* **3** (2–3), 187.
- Meyre C., De Capitani C. and Partzsch J. H. (1997) A ternary solid solution for omphacite and its application to geothermobarometry of eclogites from the middle Adula Nappe (Central Alps, Switzerland). *J. Metamorph. Geol.* **15**, 687–700.
- Meyre C., De Capitani C., Zack T. and Frey M. (1999) Petrology of high-pressure metapelites from the Adula Nappe (Central Alps, Switzerland). *J. Petrol.* **40**, 199–213.
- Möckel J. R. (1969) Structural petrology of the garnet peridotite of Alpe Arami (Ticino, Switzerland). *Leidse Geol. Med.* **42**, 61–130.
- Muramatsu Y. and Parr R. M. (1985) IAEA/RL/128: Survey of currently available reference materials for use in connection with the determination of trace elements in biological and environmental materials. *Int. Atom. Energy Agency, Vienna*.
- Muramatsu Y. and Wedepohl K. H. (1998) The distribution of iodine in the earth's crust. *Chem. Geol.* **147**, 201–216.
- Muramatsu Y., Doi T., Tomaru H., Fehn U., Takeuchi R. and Matsumoto R. (2007) Halogen concentrations in pore waters and sediments of the Nankai Trough, Japan: implications for the origin of gas hydrates. *Appl. Geochem.* **22**, 534–556.
- Nimis P. and Trommsdorff V. (2001) Revised thermobarometry of Alpe Arami and other Garnet Peridotites from the Central Alps. *J. Petrol.* **42**(1), 103–115.
- Page L., Hattori K., de Hoog J. and Okay A. (2016) Halogen (F, Cl, Br, I) behaviour in subducting slabs: a study of lawsonite blueschists in western Turkey. *Earth Planet. Sci. Lett.* **442**, 133–142.
- Page L. and Hattori K. (2017) Tracing halogen and B cycling in subduction zones based on obducted, subducted and forearc serpentinites of the Dominican Republic. *Sci. Rep.* **7**, 17776.
- Paquin J. and Altherr R. (2000) New constraints on the P-T evolution of the Alpe Arami garnet peridotite body (Central Alps, Switzerland). *J. Petrol.* **42**(6), 1119–1140.
- Pelletier L. and Müntener O. (2006) High-pressure metamorphism of the Lanzo peridotite and its oceanic cover, and some consequences for the Sesia-Lanzo zone (northwestern Italian Alps). *Lithos* **90**, 111–130.
- Pfiffner M. and Trommsdorff V. (1998) The high-pressure ultramafic-mafic-carbonate suite of Cima Lunga-Adula, Central Alps: excursions to Cima di Gagnone and Alpe Arami. *Schweiz. Mineral. Petrogr. Mitt.* **78**, 337–354.
- Pfiffner M. (1999) *Genese der hochdruckmetamorphen ozeanischen Abfolge der Cima Lunga-Einheit (Zentralalpen)* PhD thesis. ETH, Zurich.
- Philippot P., Agrinier P. and Scambelluri M. (1998) Chlorine cycling during subduction of altered oceanic crust. *Earth Planet. Sci. Lett.* **161**(1–4), 33–44.
- Piccardo G. B., Zanetti A. and Müntener O. (2007) Melt/peridotite interaction in the Southern Lanzo peridotite: field, textural and geochemical evidence. *Lithos* **94**, 181–209.
- Piccardo G. B. (2010) The Lanzo peridotite massif, Italian Western Alps: Jurassic rifting of the Ligurian Tethys. In *Petrological Evolution of the European Lithospheric Mantle*, vol. 337 (eds. M. Coltorti, H. Downes, M. Gregoire and S. Y. O'Reilly). Geological Society of London Special Publications, pp. 47–69.
- Pognante U. (1991) Petrological constraints on the eclogite- and blueschist-facies metamorphism and P-T-t paths in the Western Alps. *J. Metamorph. Geol.* **9**(1), 5–17.
- Reinecke T. (1998) Prograde high- to ultrahigh-pressure metamorphism and exhumation of oceanic sediments at Lago di Cignana, Zermatt-Saas Zone, western Alps. *Lithos* **42**, 147–189.
- Risold A. C., Trommsdorff V. and Groberty B. (2001) Genesis of ilmenite rods and palisades along humite type defects in olivine from Alpe Arami. *Contrib. Mineral. Petrol.* **140**, 619–628.
- Roberge M., Bureau H., Bolfan-Casanova N., Frost D., Raepsaet C., Surble S., Khodja H., Auzende A. and Fiquet G. (2015) Is the transition zone a deep reservoir for fluorine? *Earth Planet. Sci. Lett.* **429**, 25–32.
- Roberge M., Bureau H., Bolfan-Casanova N., Raepsaet C., Surble S., Khodja H., Auzende A., Cordier P. and Fiquet G. (2017) Chlorine in wadsleyite and ringwoodite: an experimental study. *Earth Planet. Sci. Lett.* **467**, 99–107.
- Rubatto D., Gebauer D. and Fanning M. (1998) Jurassic formation and Eocene subduction of the Zermatt-Saas-Fee ophiolites; implications for the geodynamic evolution of the Central and Western Alps. *Contrib. Mineral. Petrol.* **132**, 269–287.
- Ruzi-Hamilton L., Clay P., Burgess R., Joachim B., Ballentine C. and Turner G. (2016) Determination of halogen abundances in terrestrial and extraterrestrial samples by the analysis of noble gases produced by neutron irradiation. *Chem. Geol.* **437**, 77–87.
- Saal A. E., Hauri E. H., Langmuir C. H. and Perfit M. R. (2002) Vapour undersaturation in primitive mid-ocean-ridge basalt and the volatile content of Earth's upper mantle. *Nature* **419**, 451–455.
- Sano T., Miyoshi M., Ingle S., Banerjee N. R., Ishimoto M. and Fukuoka T. (2008) Boron and chlorine contents of upper oceanic crust: basement samples from IODP Hole 1256D. *Geochem. Geophys. Geosyst.* **9**(12), Q12O15.
- Scambelluri M., Piccardo G. B., Philippot P., Robbiano A. and Negretti L. (1997) High salinity fluid inclusions formed from recycled seawater in deeply subducted alpine serpentinite. *Earth Planet. Sci. Lett.* **148**, 485–500.
- Scambelluri M., Müntener O., Ottolini L., Pettke T. T. and Vannucci R. (2004) The fate of B, Cl and Li in the subducted oceanic mantle and in the antigorite breakdown fluids. *Earth Planet. Sci. Lett.* **222**(1), 217–234.
- Scambelluri M., Pettke T., Rampone E., Godard M. and Reusser E. (2014) Petrology and trace element budgets of high-pressure peridotites indicate subduction dehydration of serpentinized mantle (Cima di Gagnone, Central Alps, Switzerland). *J. Petrol.* **55**(3), 459–498.
- Scambelluri M., Pettke T. and Cannà E. (2015) Fluid-related inclusions in Alpine high-pressure peridotite reveal trace element recycling during subduction-zone dehydration of serpentinized mantle (Cima di Gagnone, Swiss Alps). *Earth Planet. Sci. Lett.* **429**, 45–59.
- Schilling J. G., Bergeron M. B. and Evans R. (1980) Halogens in the mantle beneath the North Atlantic. *Phil. Trans. R. Soc. Lond. A* **297**, 147–178.
- Schmidt M. W. and Poli S. (1998) Experimentally based water budgets for dehydrating slabs and consequences for arc magma generation. *Earth Planet. Sci. Lett.* **163**(1–4), 361–379.
- Shen T., Hermann J., Zhang L., Padrón-Navarta J. and Chen J. (2014) FTIR spectroscopy of Ti-chondrodite, Ti-clinohumite, and olivine in deeply subducted serpentinites and implications

- for the deep water cycle. *Contrib. Mineral. Petrol.* **167**(4), 992–1007.
- Shimizu N. and Hart S. R. (1982) Isotope fractionation in secondary ion mass spectrometry. *J. Appl. Phys.* **53**, 1303–1311.
- Spandler C., Pettke T. and Rubatto D. (2011) Internal and external fluid sources for eclogite-facies veins in the Monviso Metaophiolite, Western Alps: implications for fluid flow in subduction zones. *J. Petrol.* **52**, 1207–1236.
- Stalder R. and Ulmer P. (2001) Phase relations of a serpentine composition between 5 and 14 GPa: significance of clinohumite and phase E as water carriers into the transition zone. *Contrib. Mineral. Petrol.* **140**(6), 754–754.
- Stampfli G. M., Mosar J., Marquer D., Marchant R., Baudin T. and Borel G. (1998) Subduction and obduction processes in the Swiss Alps. *Tectonophysics* **296**, 159–204.
- Staudacher T. and Allègre C. J. (1988) Recycling of oceanic crust and sediments: the noble gas subduction barrier. *Earth Planet. Sci. Lett.* **89**, 173–183.
- Stephan T. (2001) TOF-SIMS in cosmochemistry. *Planet. Space Sci.* **49**, 859–906.
- Stephan, T. and Lyon I.C. (2013) Applications of ToF-SIMS in cosmochemistry. In *ToF-SIMS: Materials Analysis by Mass Spectrometry* (eds. J. C. Vickerman and D. Briggs), 2nd ed., IM Publications LLP and Surface Spectra Limited, pp. 709.
- Straub S. M. and Layne G. D. (2003) The systematics of chlorine, fluorine, and water in Izu arc front volcanic rocks: Implications for volatile recycling in subduction zones. *Geochim. Cosmochim. Acta* **67**(21), 4179–4203.
- Sumino H., Burgess R., Mizukami T., Wallis S., Holland G. and Ballentine C. (2010) Seawater-derived noble gases and halogens preserved in exhumed mantle wedge peridotite. *Earth Planet. Sci. Lett.* **294**(1–2), 163–172.
- Suzuki S. and Hirai S. (1992) Multielement determination in marine sediment reference material by instrumental neutron activation analysis. *Jpn. Analyst.* **41**, 163–166.
- Svensen H., Jamtveit B., Banks D. and Austrheim H. (2001) Halogen contents of eclogite facies fluid inclusions and minerals: Caledonides, western Norway. *J. metamorphic Geol.* **19**(2), 165–178.
- Symonds R. B., Rose W. I., Bluth G. J. S. and Gerlach T. M. (1994) Volcanic-gas studies: methods, results and applications. In: *Volatiles in Magmas*. Rev. Mineral. (eds. M. R. Carroll and J. R. Holloway), vol. 30, pp. 1–66.
- Tartarotti P., Martin S. and Polino R. (1986) Geological data about the ophiolitic sequences in the St. Marcel Valley (Aosta Valley). *Ophioliti* **11**(3), 343–346.
- Tartarotti P., Martin S., Monopoli B., Benciolini L., Schiavo A., Campana R. and Vigni I. (2017) Geology of the Saint-Marcel valley metaophiolites (Northwestern Alps, Italy). *J. MAPS* **13** (2), 707–717.
- Trommsdorff V. (1990) Metamorphism and tectonics in the Central Alps: The Alpine lithospheric melange of Cima Lunga and Adula. *Memorie della Societa' Geologica Italiana* **45**, 39–49.
- Trommsdorff V., Herman J., Müntener O., Pfiffner M. and Risold A. C. (2000) Geodynamic cycles of subcontinental lithosphere in the Central Alps and the Arami enigma. *J. Geodyn.* **30**, 77–92.
- Tumati S., Martin S. and Godard G. (2010) Hydrothermal origin of manganese in the high-pressure ophiolite metasediments of Praborina ore deposit (Aosta Valley, Western Alps). *Eur. J. Mineral.* **22**(4), 577–594.
- Turner G., Huneke J. C., Podosek F. A. and Wasserburg G. J. (1971) ^{40}Ar - ^{39}Ar ages and cosmic ray exposure ages of Apollo 14 samples. *Earth Planet. Sci. Lett.* **12**, 19–35.
- Ulmer P. and Trommsdorff V. (1995) Serpentine stability to mantle depths and subduction related magmatism. *Science* **268**, 858–861.
- Ulmer P. and Trommsdorff V. (1999) Phase relations of hydrous mantle subducting to 300 km. Mantle petrology: field observations and high-pressure experimentation. *Spec. Publ. Geochem. Soc.* **6**, 259–281.
- van der Klaww S. N. G. C., Reinecke T. and Stockhert B. (1997) Exhumation of ultrahigh-pressure metamorphic oceanic crust from Lago di Cignana, Piemontese zone, western Alps: the structural record in metabasites. *Lithos* **41**, 79–102.
- Yonezawa C. (1996) Multi-element determination by a cold neutron-induced prompt gamma-ray analysis. *Anal. Sci.* **12**, 605–613.

Associate editor: Wim van Westrenen